

# Altered synaptic transmission at olfactory and vomeronasal nerve terminals in mice lacking N-type calcium channel Cav2.2

Jan Weiss,<sup>1</sup> Martina Pyrski,<sup>1</sup> Petra Weissgerber<sup>2</sup> and Frank Zufall<sup>1</sup>

<sup>1</sup>Department of Physiology, University of Saarland School of Medicine, Kirrbergerstrasse, Building 58, D-66421 Homburg, Germany

<sup>2</sup>Department of Pharmacology and Toxicology, University of Saarland School of Medicine, Homburg, Germany

**Keywords:** aggression, *Cacna1b*, channelopathy, olfactory plasticity,  $\omega$ -conotoxin GVIA

## Abstract

We investigated the role of voltage-activated calcium (Cav) channels for synaptic transmission at mouse olfactory and vomeronasal nerve terminals at the first synapse of the main and accessory olfactory pathways, respectively. We provided evidence for a central role of the N-type Cav channel subunit Cav2.2 in presynaptic transmitter release at these synapses. Striking Cav2.2 immunoreactivity was localised to the glomerular neuropil of the main olfactory bulb (MOB) and accessory olfactory bulb (AOB), and co-localised with presynaptic molecules such as bassoon. Voltage-clamp recordings of sensory nerve-evoked, excitatory postsynaptic currents (EPSCs) in mitral/tufted (M/T) and superficial tufted cells of the MOB and mitral cells of the AOB, in combination with established subtype-specific Cav channel toxins, indicated a predominant role of N-type channels in transmitter release at these synapses, whereas L-type, P/Q-type, and R-type channels had either no or only relatively minor contributions. In *Cacna1b* mutant mice lacking the Cav2.2 ( $\alpha 1B$ ) subunit of N-type channels, olfactory nerve-evoked M/T cell EPSCs were not reduced but became blocker-resistant, thus indicating a major reorganisation and compensation of Cav channel subunits as a result of the Cav2.2 deletion at this synapse. Cav2.2-deficient mice also revealed that Cav2.2 was critically required for paired-pulse depression of olfactory nerve-evoked EPSCs in M/T cells of the MOB, and they demonstrated an essential requirement for Cav2.2 in vomeronasal nerve-evoked EPSCs of AOB mitral cells. Thus, *Cacna1b* loss-of-function mutations are unlikely to cause general anosmia but *Cacna1b* emerges as a strong candidate in the search for mutations causing altered olfactory perception, such as changes in general olfactory sensitivity and altered social responses to chemostimuli.

## Introduction

Investigations into the genetic basis of sensory deficits such as blindness, deafness, and pain disorders have revealed a growing list of mutations in genes encoding ion channels, specifically voltage-activated sodium (Nav) and calcium (Cav) channels, thereby providing major insights into channelopathy-associated disorders and the complex functions of ion channel mutations affecting sensory perception (Cregg *et al.*, 2010; Striessnig *et al.*, 2010; Michalakis *et al.*, 2014; Waxman & Zamponi, 2014). By contrast, progress in understanding channelopathy-associated dysfunction in the olfactory system has been slow (Feldmesser *et al.*, 2007; Karstensen & Tommerup, 2012). Recently, we have shown that loss-of-function mutations in *Scn9a*, encoding the sodium channel Nav1.7, cause a loss of the sense of smell (congenital general anosmia) in both mice and humans (Weiss *et al.*, 2011). These results also revealed a loss

of synaptic transfer at the first synapse in the main olfactory pathway of conditional Nav1.7-deficient mice (Weiss *et al.*, 2011). On the basis of these findings, we proposed that the first synapse in the olfactory system could be a rewarding target in the search for additional anosmia-related gene defects (Zufall *et al.*, 2012). Very little is still known about the contribution of ion channels to action potential propagation and transmitter release at this synapse and many of the molecular components involved in the presynaptic release machinery remain to be identified.

Here we perform a systematic analysis of presynaptic Cav channels at axon terminals of olfactory sensory neurons (OSNs) in the main olfactory bulb (MOB) of mice. For comparison, we also analyse Cav channels at axon terminals of vomeronasal sensory neurons (VSNs) in the accessory olfactory bulb (AOB). A given OSN or VSN recognises and transduces molecular cues (odorants and pheromones) at its dendritic ending and transmits this information via a single axon into glomeruli at the surface of the MOB or AOB, respectively, where axon terminals form synapses onto second-order neurons (Munger *et al.*, 2009). Cav channels play pivotal roles in the control of neurotransmitter release (for a review, see Kamp

Correspondence: Frank Zufall, as above.  
E-mail: frank.zufall@uks.eu

Received 13 May 2014, revised 31 July 2014, accepted 4 August 2014

*et al.*, 2012). Ten mammalian pore-forming  $\alpha 1$  subunits have been cloned and shown to be differentially expressed. They are subdivided on the basis of their functional properties into L-type (Cav1.1–1.4), P/Q-type (Cav2.1), N-type (Cav2.2), R-type (Cav2.3), and T-type (Cav 3.1–3.3) (Catterall *et al.*, 2005b; Striessnig & Koschak, 2008). In identified OSNs, gene expression profiling has found four  $\alpha 1$  subunit genes (*Cacna1b*, *Cacna1d*, *Cacna1f* and *Cacna1h*) (Nickell *et al.*, 2012). With few exceptions (Isaacson & Strowbridge, 1998; Wachowiak *et al.*, 2005), very little is still known about the presynaptic functions of Cav channels at mammalian OSN axon terminals. No gene knockout models have been used in these experiments and no studies have been reported concerning the function of presynaptic Cav channels at VSN axon terminals. We present a combination of physiological, pharmacological, and immunohistochemical analyses in wild-type mice and mice with a mutation in *Cacna1b* causing a genetic ablation of the  $\alpha 1B$  subunit (Cav2.2) of N-type Cav channels (Ino *et al.*, 2001).

## Materials and methods

### Animals

All procedures were approved by the Institutional Animal Care and Use Committee of the University of Saarland School of Medicine and were in accordance with the laws for animal experiments issued by the German Government. Experiments were performed on 3–6-week-old mice of both sexes. We employed three different genotypes: (i) wild-type mice (C57BL/6J, denoted as B6); (ii) mice harbouring a targeted, global deficiency of the *Cacna1b* gene, thus lacking the  $\alpha 1B$  subunit (Cav2.2) of the N-type Cav channel (denoted as Cav2.2<sup>-/-</sup> mice; Ino *et al.*, 2001); and (iii) their heterozygous littermate controls, denoted as Cav2.2<sup>+/-</sup> mice. The background of the Cav2.2 mutant mice was B6 (Ino *et al.*, 2001). Mice were housed in microisolator cages on a 12 : 12-h light/dark cycle with food and water available *ad libitum*. Cav2.2 genotypes were verified by polymerase chain reaction from tail-tip biopsies using wild-type forward (5'-TGGCACCTTATGCCTTGCACGGTGCCTGCG-3'), mutant forward (5'-GCCTGCTTGCCGAATATCATGGTGG AAAAT-3'), and reverse (5'-GGTCGATGCTTGC GGGGACC CGTTGGGA-3') primers.

### Expression of Cav2.2, bassoon, olfactory marker protein, vesicular glutamate transporter type 2, and tyrosine hydroxylase

The perfusion of mice, preparation of mouse olfactory tissues and immunohistochemistry followed previously described methods (Weiss *et al.*, 2011). Briefly, following anaesthesia [165 mg/kg body weight ketamine (Pharmacia GmbH, Berlin, Germany) and 11 mg/kg body weight xylazine (Bayer Health Care, Leverkusen, Germany)], mice were transcardially perfused with phosphate-buffered saline (PBS), followed by 2% (w/v) paraformaldehyde in PBS. The olfactory bulbs (OBs) were dissected, incubated overnight in 30% sucrose in PBS at 4 °C, embedded in O.C.T. (Tissue-Tek), and snap-frozen in a dry ice/2-methylbutane bath. Frozen tissue sections (12–30  $\mu$ m) were collected on a cryostat (HM525; Microm, Walldorf, Germany) and subjected to immunohistochemistry. The primary antibodies used were: olfactory marker protein (1 : 2000, goat polyclonal; gift of F. Margolis, University of Maryland School of Medicine, MD, USA), vesicular glutamate transporter type 2 (1 : 2000, rabbit polyclonal, cat. no. 135403; Synaptic Systems, Göttingen, Germany), Cav2.2 (1 : 100, rabbit polyclonal, cat. no.

ACC-002, lot no. AN-31; Alomone Labs, Jerusalem, Israel), bassoon (1 : 500, mouse monoclonal, cat. no. AB82958; Abcam, Cambridge, UK), and tyrosine hydroxylase (TH) (1 : 2000, mouse monoclonal, cat. no. 22941; ImmunoStar, Hudson, WI, USA). The incubation of tissue sections in primary antibody was overnight at 4 °C, and all other procedures were conducted at room temperature (20 °C). Secondary antibodies were: Alexa-Fluor 488-conjugated donkey anti-goat, Alexa-Fluor 488 goat anti-rabbit, Alexa-Fluor 555 donkey anti-rabbit, and Alexa-Fluor 555 donkey anti-mouse (1 : 1000; Invitrogen, Darmstadt, Germany). TH expression was detected using the avidin/biotin amplification method (Vectastain ABC-Elite; Vector Laboratories, Burlingame, CA, USA). Free-floating cryosections of the OBs (30  $\mu$ m, coronal plane) were sequentially incubated for 10 min in 3% H<sub>2</sub>O<sub>2</sub>/PBS, 1 h in blocking solution (PBS, pH 7.4, 4% normal horse serum, 0.3% Triton-X 100), overnight at 4 °C in primary mouse anti-TH antibody diluted in blocking solution, 1 h in biotinylated horse anti-mouse IgG (1 : 400; Vector Laboratories), and 90 min in avidin/biotin horseradish peroxidase complex (Vector Laboratories). Immunoreactivity was visualised with 0.05 g/L 3,3'-diaminobenzidine (Sigma-Aldrich, Taufkirchen, Germany) and 0.015% H<sub>2</sub>O<sub>2</sub> in PBS. Bright-field images were acquired on a BX61 microscope attached to a DP71 camera (Olympus) and minimally adjusted in contrast and brightness using Photoshop Elements 10 (Adobe Photoshop).

### Electrophysiology

Mice were deeply anaesthetised with CO<sub>2</sub>, killed by decapitation, and the OBs were rapidly dissected in ice-cold oxygenated (95% O<sub>2</sub>, 5% CO<sub>2</sub>) solution containing the following (in mM): 83 NaCl, 26.2 NaHCO<sub>3</sub>, 1 NaH<sub>2</sub>PO<sub>4</sub>, 2.5 KCl, 3.3 MgCl<sub>2</sub>, 0.5 CaCl<sub>2</sub> and 70 sucrose, pH 7.3 (osmolarity, 300 mOsm/L). The tissue was mounted on a vibratome (VT1000S; Leica Microsystems, Nussloch, Germany) and horizontal MOB or oblique/horizontal AOB slices (275  $\mu$ m thick) were cut in the same solution. Slices were first stored at 34–36 °C for 30 min in standard extracellular solution and afterwards at room temperature until use. The extracellular solution contained the following (in mM): 125 NaCl, 25 NaHCO<sub>3</sub>, 2.5 KCl, 1.25 NaH<sub>2</sub>PO<sub>4</sub>, 1 MgCl<sub>2</sub>, 2 CaCl<sub>2</sub> and 25 glucose (continuously bubbled with 95% O<sub>2</sub>, 5% CO<sub>2</sub>). Tissue slices were placed in the recording chamber and superfused at a rate of approximately 2 mL/min (gravity flow) with sodium hydrogen carbonate-buffered extracellular solution bubbled with carbogen (95% O<sub>2</sub>, 5% CO<sub>2</sub>). Cells were visualised in intact tissue slices with a 40 $\times$  water immersion objective lens (Olympus Optical) using infrared-optimised differential interference contrast optics and fluorescent illumination and a green fluorescent protein filter set attached to the microscope to elucidate the morphology of lucifer yellow-filled mitral and tufted cells (BX50WI; Olympus) (Ukhanov *et al.*, 2007).

Slice recordings were carried out at room temperature using an EPC-9 automated patch-clamp amplifier (HEKA Elektronik, Lambrecht, Germany) and PULSE 8.11 software as described previously (Weiss *et al.*, 2011). Patch pipettes were pulled from borosilicate glass tubing (World Precision Instruments, Germany). The signals were filtered using an eight-pole Bessel filter built into the EPC-9 amplifier and digitised at a frequency  $\geq$  filter cut-off frequency (VR-10B; Instrutech Corp.). The sampling rate during all recordings was 10 kHz. The recording pipettes had resistances of 3–6 M $\Omega$ . Cells were voltage-clamped in the whole-cell patch-clamp mode. Cell types in the MOB were defined on the basis of the following criteria. Mitral/tufted (M/T) cells had an ellipsoid-shaped cell body with a diameter of > 10  $\mu$ m, were located in the mitral cell layer and had

input resistances of 200–500 M $\Omega$ . We did not discriminate between mitral cells and tufted cells within the group of M/T cells. M/T cells were filled with lucifer yellow during the recording and were afterwards visually inspected using fluorescent illumination. ‘Superficial’ tufted cells (sTCs; Gire *et al.*, 2012) were recorded in close proximity to the glomerular layer and identified by their ellipsoid-shaped soma and the presence of lateral dendrites, observed by lucifer yellow fluorescence. AOB mitral cells were located in the intermediate external plexiform layer of the AOB and were defined by their large (> 10- $\mu$ m) ellipsoid- or triangular-shaped somata and their large glomerular dendrites targeting several glomeruli.

The intracellular solution contained (in mM): 140 CsCl, 1 EGTA, 10 HEPES, 2 ATP Na-salt, 1 GTP Mg-salt, 5 QX-314 (a lidocaine derivative; Sigma-Aldrich), 0.1 lucifer yellow and 0.4 neurobiotin (Vector Laboratories) (pH 7.1; osmolarity, 290 mOsm). M/T cells and sTCs were voltage clamped to  $-60$  mV. The input resistances were about 200–500 M $\Omega$  and series resistances were 7–20 M $\Omega$ , and were left uncompensated in most recordings. Mitral cells in the AOB had higher input resistances (600 M $\Omega$  to > 1 G $\Omega$ ). The theoretical liquid junction potential between intracellular and extracellular compartments was calculated to be 4.1 mV and was not corrected.

After establishing a whole-cell recording, we waited for at least 3 min before data acquisition began to allow for equilibration of intracellular solution into the dendrites. We stimulated the olfactory or vomeronasal nerve (VN) layers through a glass electrode (1–1.5 M $\Omega$ ) filled with extracellular solution and connected to an Isolated Pulse Stimulator Model 2100 (A-M Systems Instruments, USA). The stimulus intensity was usually 100 V, except for stimulus intensity vs. amplitude experiments (10–100 V), stimulus duration was 100  $\mu$ s/1 ms, and stimuli were repeated every 2 min. After the second stimulation, Ca<sup>2+</sup> channel blockers such as 100  $\mu$ M CdCl<sub>2</sub>, 10  $\mu$ M nifedipine, 200 nM SNX-482, 200 nM  $\omega$ -agatoxin IVA, 2  $\mu$ M  $\omega$ -conotoxin GVIA, 10  $\mu$ M mibefradil, or 500  $\mu$ M NiCl<sub>2</sub> were bath-applied for 8 min, followed by a washout period lasting at least another 8 min. In some recordings ( $n = 14$ ), bicuculline (10  $\mu$ M) was used to block GABAergic inhibitory postsynaptic currents. Because there was no difference between bicuculline-treated and non-treated slices for Ca<sup>2+</sup> channel pharmacology, we pooled datasets. The  $\alpha$ -amino-3-hydroxy-5-methyl-4-isoxazolepropionic acid receptor blocker 6-cyano-7-nitroquinoxaline-2,3-dione disodium was used at 10  $\mu$ M. A blocker of gap junctions, carbenoxolone, was applied at a concentration of 300  $\mu$ M. All pharmacological agents were prepared as concentrated aliquots and stored at  $-20$  °C. The peptide toxins  $\omega$ -agatoxin IVA,  $\omega$ -conotoxin GVIA and SNX-482 were from PeptaNova (Sandhausen, Germany); CdCl<sub>2</sub>, nifedipine, mibefradil, 6-cyano-7-nitroquinoxaline-2,3-dione disodium, bicuculline, and carbenoxolone were from Sigma-Aldrich; and NiCl<sub>2</sub> was from Roth (Karlsruhe, Germany). For each experiment, stock solutions were freshly diluted in extracellular solution.

Following patch-clamp recording, OB slices containing lucifer yellow- and neurobiotin-filled neurons were fixed for 30–60 min with 4% (w/v) paraformaldehyde in PBS (pH 7.4, at room temperature) and washed in PBS several times. The slices were incubated in 4% normal horse serum (v/v), 0.5% (v/v) Triton X-100 in PBS with Streptavidin 488 (1 : 500; Molecular Probes, Göttingen, Germany) at room temperature for 1–3 h. Finally, OB slices were washed in PBS several times. Confocal photomicrographs of injected M/T and tufted cells were taken with a confocal laser scanning microscope (DM6000CFS; Leica Microsystems, Heidelberg, Germany) using a 20 $\times$  water immersion objective. Stacks of confocal images (z-stack step size 1  $\mu$ m) were projected onto a single image plane. Acquired

confocal images were further used to reconstruct some of the injected cells using NEUROMANTIC software (<http://www.reading.ac.uk/neuromantic/>).

### Data analysis

All electrophysiological data were analysed using IGOR PRO software (WaveMetrics) and Excel (Microsoft). The delay of excitatory postsynaptic currents (EPSCs) was defined as the time interval between the beginning of the stimulation artefact and the time point at which the current first deviated from baseline. EPSC duration was quantified by measuring the time from the beginning of the stimulus artefact until inward currents reached baseline again. For pharmacological experiments, amplitudes of evoked EPSCs were assessed and each value was normalised to the value obtained by the second electrical stimulation. For paired-pulse ratios, EPSC peak amplitudes were normalised to the conditioning response (EPSC<sub>2</sub> : EPSC<sub>1</sub>). In AOB experiments with Cav2.2<sup>-/-</sup> mice, we discriminated between type 1 and type 2 mitral cell responses on the basis of EPSC peak amplitude ratios in a given cell that were evoked by two distinct stimulation protocols (EPSC<sub>short pulse</sub> : EPSC<sub>tetanic</sub>). Cells exhibiting a ratio > 0.25 were grouped into type 1 cells and cells with a ratio < 0.25 were classified as type 2 cells. The Student's *t*-test was used for measuring the significance of difference between two distributions (\* $P < 0.05$ ; \*\* $P < 0.005$ ; \*\*\* $P < 0.0005$ ). Data are expressed as means  $\pm$  SEM.

## Results

### Olfactory nerve-evoked excitatory postsynaptic currents in mitral/tufted cells of the main olfactory bulb

To investigate Cav channel function underlying transmitter release from olfactory nerve (ON) terminals, we recorded postsynaptic currents of voltage-clamped ( $-60$  mV) M/T and ‘superficial’ tufted cells (sTCs) in horizontal mouse OB slices (Fig. 1A) in response to brief electrical stimulation of OSN axons that were located in the ON layer of the MOB. In most experiments, stimulating electrodes were placed at a distance of  $\geq 50$   $\mu$ m from the target glomerulus (Fig. 1A, and see below). Results are based on recordings from 144 M/T cells and 16 sTCs in 52 mice (25 B6, 14 Cav2.2<sup>+/-</sup>, and 13 Cav2.2<sup>-/-</sup> mice). In B6 mice, ON stimulation caused activation of characteristic inward currents in M/T cells that could be blocked in a reversible manner by bath-applied Cd<sup>2+</sup> (100  $\mu$ M) (Fig. 1B) ( $n = 4$ ) or the  $\alpha$ -amino-3-hydroxy-5-methyl-4-isoxazolepropionic acid receptor blocker 6-cyano-7-nitroquinoxaline-2,3-dione disodium (10  $\mu$ M) (Fig. 1C) ( $n = 8$ ), indicating that the currents were largely caused by synaptic release of glutamate. ON-evoked EPSCs in M/T cells had amplitudes between  $-100$  pA and  $-1.5$  nA (mean  $-397 \pm 48$  pA;  $n = 44$ ) and lasted typically between 0.2 and 3 s (mean  $1.13 \pm 0.02$  s;  $n = 12$ ). The delay between electrical stimulation and inward current onset in M/T cells ranged between 1.9 and 3.1 ms (mean  $2.5 \pm 0.2$  ms,  $n = 15$ ), consistent with monosynaptic activation from OSNs onto M/T cells (Najac *et al.*, 2011; Gire *et al.*, 2012). Examples for this rapid activation at higher temporal resolution are shown in Fig. 1D. To minimise the possibility that M/T cell activation resulted from direct electrical stimulation of tufted cell dendrites, we placed the stimulation electrode at a distance of  $\geq 200$   $\mu$ m (in some cases up to 500  $\mu$ m) from the target glomerulus and applied carbenoxolone (300  $\mu$ M) (Hayar *et al.*, 2005; Tyler *et al.*, 2007) in order to prevent shunting by gap junctions (Christie *et al.*, 2005; Zufall, 2005; Gire *et al.*, 2012). With

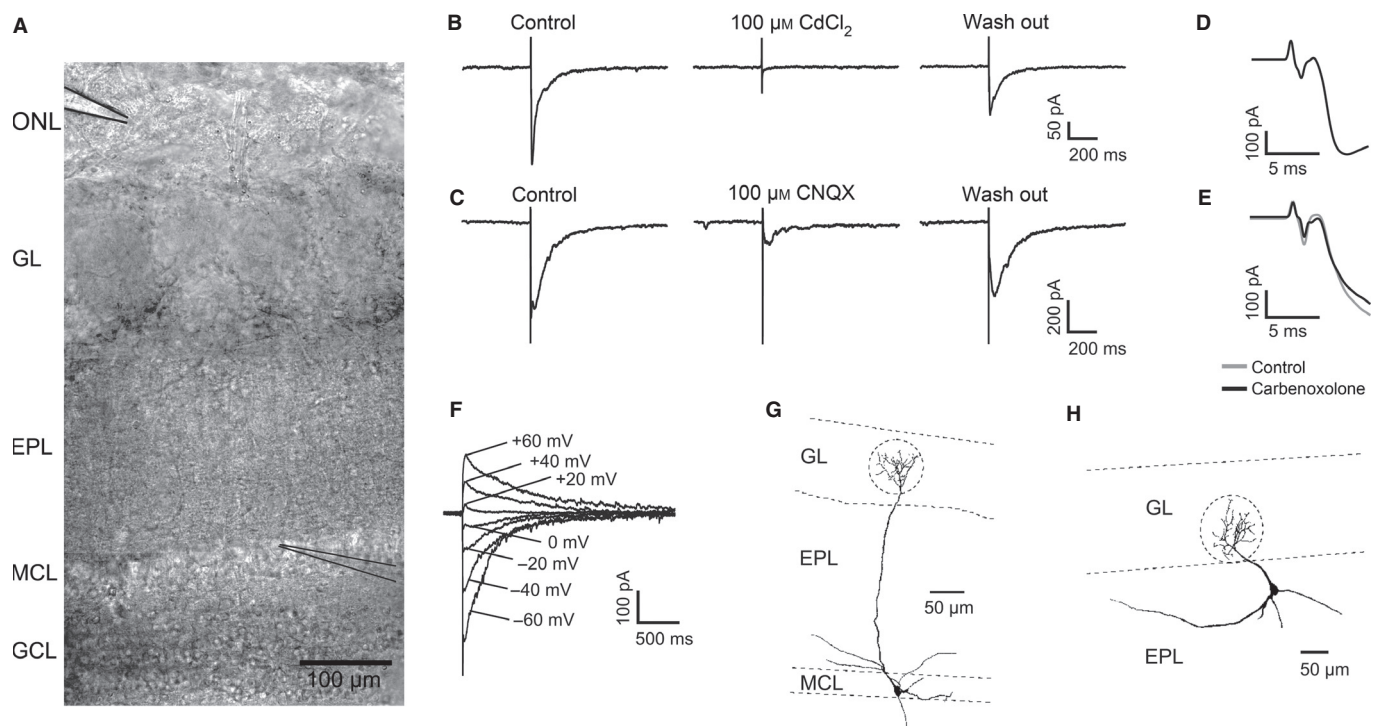


FIG. 1. Properties of ON-evoked EPSCs. (A) Micrograph of the MOB slice preparation (20 $\times$  water immersion objective) showing the location of the recording pipette in the MCL and of the stimulation pipette in the ON layer (ONL). GL, glomerular layer; EPL, external plexiform layer; MCL, mitral cell layer; GCL, granule cell layer. (B) Time course of ON-evoked M/T cell EPSCs recorded under control conditions, in the presence of  $\text{Cd}^{2+}$  (100  $\mu\text{M}$ ), and after washout of the blocker. (C) Time course of ON-evoked M/T cell EPSCs recorded under control conditions, in the presence of 6-cyano-7-nitroquinoxaline-2,3-dione disodium (CNQX) (10  $\mu\text{M}$ ), and after washout of the drug. (D) ON-evoked M/T cell EPSCs averaged from five independent experiments and plotted at expanded time resolution to show the delay and initial rising phase of the currents. Stimulating electrodes were placed at a distance of  $\geq 50 \mu\text{m}$  from the target glomerulus. (E) ON-evoked M/T cell EPSCs averaged from six independent experiments before (control, grey trace) and after (black trace) application of 300  $\mu\text{M}$  carbenoxolone. Stimulating electrodes were placed at a distance of  $\geq 200 \mu\text{m}$  from the target glomerulus. (F) EPSCs recorded in an M/T cell at different holding potentials (in 20-mV increments between  $-60$  and  $60$  mV). Reconstructions of a recorded M/T cell (G) and an sTC (H) filled with lucifer yellow and neurobiotin.

these precautions, we observed the same short EPSC latencies and rapid early rise time kinetics (Fig. 1E) ( $n = 6$ ). The delay between electrical stimulation and inward current onset in M/T cells treated with 300  $\mu\text{M}$  carbenoxolone ranged between 2.6 and 3.7 ms (mean  $3.2 \pm 0.15$  ms,  $n = 6$ ). These values were not significantly different to those from control responses ( $t$ -test,  $t_{19} = 1.76$ ,  $P = 0.09$ ) or to onset delays before carbenoxolone treatment (paired  $t$ -test,  $t_{10} = 1.27$ ,  $P = 0.23$ ). EPSC amplitudes depended on the membrane holding potential, with a reversal potential between 0 and 10 mV (Fig. 1F) ( $n = 10$ ), indicating appropriate voltage control along the primary dendritic tuft during the recording and only minor contributions of inward currents via gap junctions from surrounding mitral cells or external tufted cells (De Saint Jan *et al.*, 2009; Gire *et al.*, 2012). Thus, ON electrical stimulation under our conditions elicited EPSCs that were likely to include monosynaptic components and depended on Cav channels and glutamate release.

Neurons were filled with lucifer yellow and neurobiotin during these recordings and their cell morphology was analysed in detail using posthoc confocal microscopy (12 M/T cells and four sTCs). Figure 1G shows a reconstructed M/T cell with its primary dendritic tuft targeting a single glomerulus and some lateral dendrites that were often truncated during the slicing procedure. The reconstructed morphology of an sTC is shown in Fig. 1H. In contrast to M/T cells, these neurons were characterised by somata located in the external plexiform layer of the MOB, in close proximity to the glomerular layer.

### Critical role of N-type voltage-activated calcium channels

The N-type Cav channels are known to mediate transmitter release of GABAergic and glutamatergic neurons in many parts of the mammalian central nervous system (Kamp *et al.*, 2012) and some glutamatergic sensory neurons of peripheral pain pathways (Zamponi *et al.*, 2009).  $\omega$ -conotoxin GVIA is a potent, selective, and irreversible inhibitor of such N-type channels (Catterall *et al.*, 2005a). We hypothesised that this channel subtype could underlie transmitter release at OSN axon terminals and tested the effect of  $\omega$ -conotoxin GVIA on ON-evoked EPSCs in M/T cells and sTCs (Fig. 2). Application of  $\omega$ -conotoxin GVIA (2  $\mu\text{M}$ ) reduced the peak amplitudes of postsynaptic currents to  $18 \pm 2\%$  of control in M/T cells ( $n = 15$ ) (Fig. 2C) ( $t$ -test,  $t_{27} = 2.6$ – $4.7$ ,  $P < 0.018$  for stimulations 5–10), whereas current amplitudes in untreated control cells ( $n = 14$ ) remained stable over time (Fig. 2C, grey) ( $91 \pm 1.6\%$  of control). A representative example is shown in Fig. 2A, with EPSCs recorded before (left), during (middle) and after (right) exposure to  $\omega$ -conotoxin GVIA.

The MOB mitral cells receive direct input from OSNs (Shepherd *et al.*, 2004; Najac *et al.*, 2011). It has been shown recently that additional feedforward excitation from external tufted and/or tufted cells contributes to mitral cell activation (Carlson *et al.*, 2000; Najac *et al.*, 2011; Gire *et al.*, 2012). To exclude the possibility that  $\omega$ -conotoxin GVIA affected only transmission at dendrodendritic synapses between sTCs and mitral cells (Najac

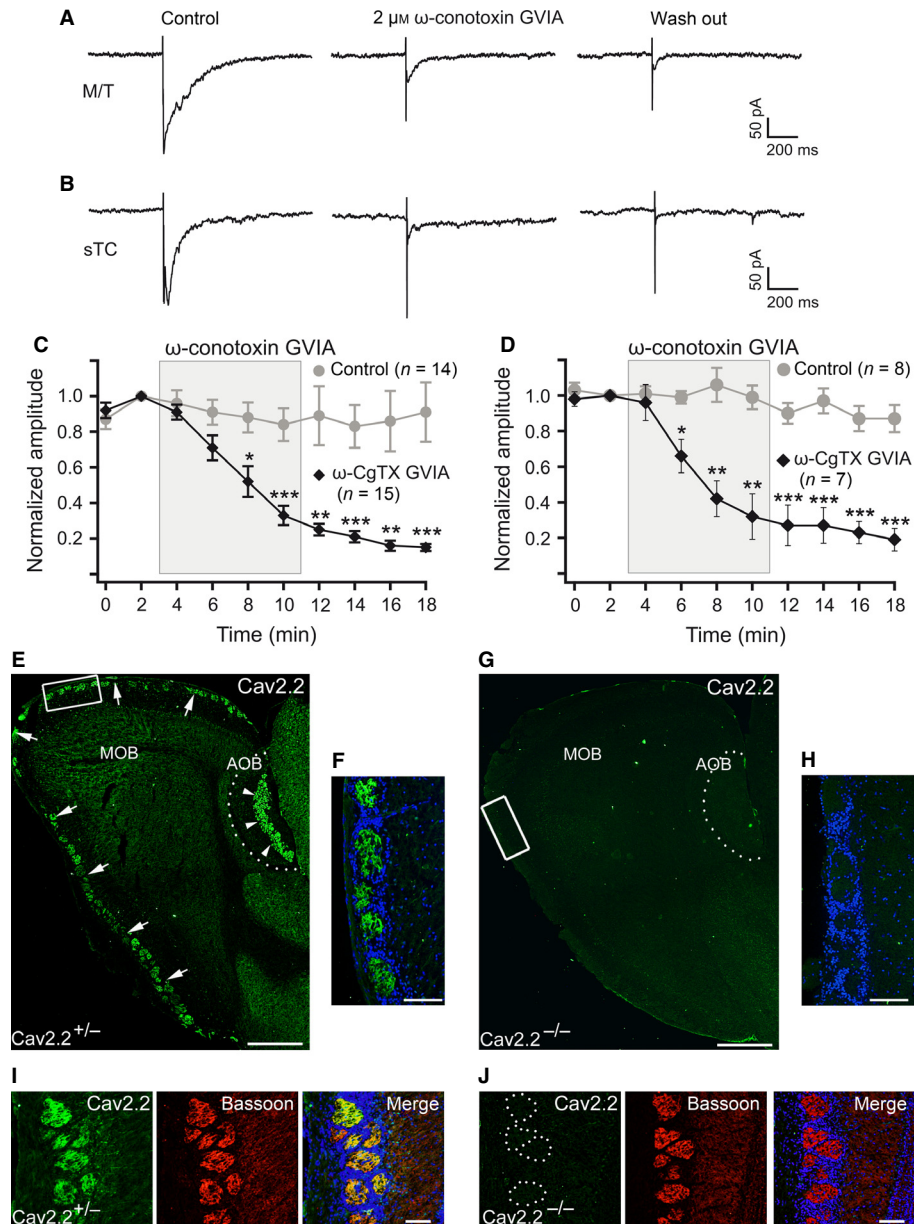


FIG. 2. Essential role of N-type Cav channels in ON-evoked EPSCs of M/T cells and sTCs. (A) EPSCs of an M/T cell before (left), during (middle) and after (right) treatment with  $\omega$ -conotoxin GVIA ( $2 \mu\text{M}$ ). (B) EPSCs of an sTC before, during and after treatment with  $\omega$ -conotoxin GVIA ( $2 \mu\text{M}$ ). (C) Normalised peak EPSC amplitudes of M/T control cells ( $n = 14$ , grey) vs. cells treated with  $\omega$ -conotoxin (CgTX) GVIA ( $n = 15$ , black). (D) Normalised peak EPSC amplitudes of sTCs [control cells ( $n = 8$ , grey),  $\omega$ -conotoxin GVIA-treated cells ( $n = 7$ , black)]. Peak amplitudes of EPSCs were normalised to the response evoked by the second stimulus. Error bars represent means  $\pm$  SEM. \* $P < 0.05$ ; \*\* $P < 0.005$ ; \*\*\* $P < 0.0005$ . (E, F) Cav2.2 immunoreactivity (green) detected in the OB ( $14 \mu\text{m}$ , sagittal plane) of a Cav2.2<sup>+/-</sup> mouse is present in the glomeruli of the MOB (arrows) and the glomeruli of the AOB (dotted line, arrowheads). (F) Inset magnification (box in E) of Cav2.2 immunoreactivity (green) in the MOB glomeruli counterstained with nuclear dye (blue, Hoechst 33342). (G) In contrast, Cav2.2 immunoreactivity is absent in both the MOB and in the glomeruli of the AOB (dotted line) of a Cav2.2<sup>-/-</sup> mouse. (H) Inset magnification of the box in G, counterstained with nuclear dye (blue) depicting the extent of MOB glomeruli that are devoid of any Cav2.2 immunoreactivity (green). (I) Cav2.2 (left, green) co-localises with the presynaptic marker bassoon (middle, red) in the MOB glomeruli (orange merge, right) of a Cav2.2<sup>+/-</sup> mouse. (J) In the Cav2.2<sup>-/-</sup> mouse, Cav2.2 immunoreactivity is absent in MOB glomeruli (left, dotted circles), whereas bassoon (red, middle) shows prominent staining that is restricted to the glomerular layer as depicted by nuclear counterstaining (right, merge). Scale bars – 500  $\mu\text{m}$  (E, G); 100  $\mu\text{m}$  (F–J).

*et al.*, 2011), we performed further recordings on sTCs. ON-evoked EPSCs in sTCs were similar to M/T cell responses. They possessed stimulation latencies of  $2.8 \pm 0.16$  ms (ranging from 1.6 to 3.7 ms), amplitudes of  $-451 \pm 96$  pA, and lasted between 200 ms and 3 s (mean  $0.91 \pm 0.024$  s,  $n = 15$ ). Consistent with results from M/T cells, we found that  $\omega$ -conotoxin GVIA ( $2 \mu\text{M}$ ) also inhibited synaptic responses of sTCs to  $19 \pm 6\%$  (Fig. 2B and D; *t*-test,  $t_{13} = 3.2\text{--}6.2$ ,  $P < 0.007$  for stimulations 4–10),

whereas EPSC amplitudes of untreated sTCs persisted over time with relatively little run-down (Fig. 2D, grey) ( $87 \pm 7\%$  residual current). Thus,  $\omega$ -conotoxin GVIA strongly decreased ON-evoked EPSCs of both cell types and the extent of this effect was nearly identical in both cases. We therefore conclude that mouse OSNs employ primarily N-type Cav channels to regulate the release of glutamate from their axon terminals for fast synaptic transmission.

Consistent with these results, we found that Cav2.2 protein was present in the MOB of control mice. Using fluorescence immunohistochemistry in Cav2.2<sup>+/-</sup> mice, we detected robust Cav2.2 staining in the glomerular neuropil that included the presynaptic OSN boutons, but not in the ON layer containing axons from OSNs (Fig. 2E and F). Cav2.2 staining in wild-type mice gave the same result (not shown). Importantly, Cav2.2 immunoreactivity was absent in the glomeruli of Cav2.2<sup>-/-</sup> mice, thus verifying the specificity of the antibody staining (Fig. 2G and H). In addition, we performed double-labelling immunohistochemistry for Cav2.2 and bassoon, a scaffolding protein of the presynaptic cytomatrix at the active zone (tom Dieck *et al.*, 1998; Dani *et al.*, 2010). Our results showed that, in Cav2.2<sup>+/-</sup> mice, Cav2.2 and bassoon immunoreactivity co-localised in the glomeruli of the MOB (Fig. 2I). In the Cav2.2<sup>-/-</sup> mice, bassoon immunoreactivity was unchanged. Together, these results suggested that Cav2.2 is likely to play a role in presynaptic transmitter release at the first synapse of the main olfactory pathway. Furthermore, we found striking Cav2.2 immunoreactivity in virtually all glomeruli of the AOB in Cav2.2<sup>+/-</sup> mice (Fig. 2E). As in the MOB, this labelling was absent in Cav2.2<sup>-/-</sup> mice (Fig. 2G) but bassoon immunoreactivity was unchanged (not shown), indicating that Cav2.2 could also play important roles in presynaptic transmitter release of axon terminals from VSNs in the accessory olfactory system.

#### Minor contributions of L-type, P/Q-type, and R-type voltage-activated calcium channels

Despite a striking inhibitory effect of  $\omega$ -conotoxin GVIA (Fig. 2), there was still a considerable residual current left in most recordings

after exposure to this antagonist. To explore potential contributions of other Cav channel subtypes to fast synaptic transfer at OSN axon terminals, we recorded ON-evoked EPSCs in M/T cells and tested the effects of several other well-established Cav channel inhibitors. In the mammalian auditory and visual systems, L-type Cav channels (Cav1.1–1.4) are specifically involved in transmitter release at several ribbon but also at conventional synapses (e.g. hair cells, amacrine cells; Platzer *et al.*, 2000; Habermann *et al.*, 2003). We applied the L-type Cav channel blockers nifedipine (10  $\mu$ M) (Fig. 3A) and verapamil (10  $\mu$ M, not shown) but found virtually no reduction of ON-evoked M/T cell EPSCs under these conditions, indicating that L-type Cav channels were not involved in transmitter release from OSN axon terminals (Fig. 3B) ( $106 \pm 7\%$  of control at last stimulation of nifedipine treatment;  $n = 11$ ;  $t$ -test,  $t_{23} = 0.0015$ – $2.001$ ,  $P = 0.06$ – $0.99$ ).

The P/Q-type Cav channels containing the Cav2.1 subunit play a major role at many glutamatergic synapses in the central nervous system (Striessnig & Koschak, 2008). We therefore examined the effect of  $\omega$ -agatoxin IVA, a Cav2.1 subunit-specific inhibitor (Catterall *et al.*, 2005a), on ON-evoked EPSCs in M/T cells (Fig. 3C and D). In the presence of  $\omega$ -agatoxin IVA (200 nM), there was a tendency for slightly reduced EPSC peak amplitudes, an effect that continued after washout of the antagonist. Overall, however, we found no statistically significant difference compared with untreated slices (Fig. 3C and D) ( $79 \pm 5\%$  of control at last stimulation;  $t$ -test,  $t_{27} = 0.20$ – $1.96$ ,  $P = 0.06$ – $0.83$ ). To investigate this point further, we also applied  $\omega$ -agatoxin IVA (200 nM) together with  $\omega$ -conotoxin GVIA (2  $\mu$ M) (data not shown). This combination of peptide toxins inhibited EPSC peak amplitudes in three M/T cells to

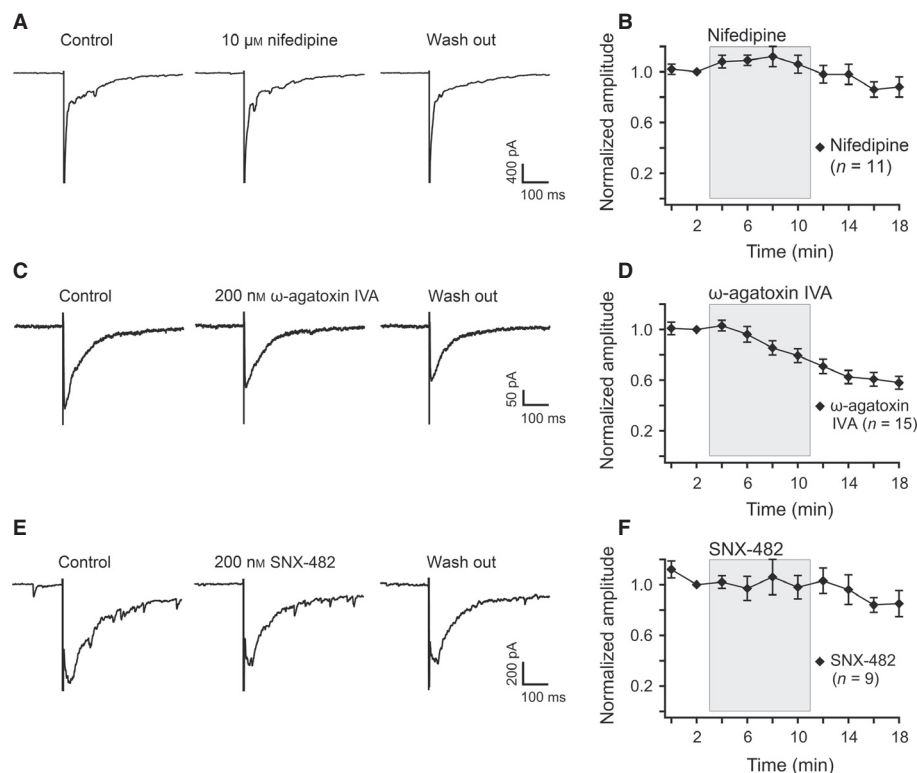


FIG. 3. Minor contributions of L-type, P/Q-type, and R-type Cav channels. (A) EPSCs of an M/T cell before (left), during (middle), and after (right) treatment with nifedipine (10  $\mu$ M). (B) Effect of nifedipine (10  $\mu$ M) on normalised EPSC peak amplitudes plotted over time ( $n = 11$ ). (C) EPSCs of an M/T cell before, during, and after treatment with  $\omega$ -agatoxin IVA (200 nM). (D) Effect of  $\omega$ -agatoxin IVA on normalised EPSC peak amplitudes ( $n = 15$ ). (E) EPSCs of an M/T cell before, during, and after treatment with SNX-482 (200 nM). (F) Effect of SNX-482 on normalised EPSC peak amplitudes ( $n = 9$ ). Error bars represent means  $\pm$  SEM.

18 ± 7% of control, similar to the inhibition of  $\omega$ -conotoxin GVIA alone (compare with Fig. 2C). Thus, the residual EPSCs that we observed in the presence of  $\omega$ -conotoxin GVIA did not seem to be caused by the activity of Cav2.1.

The Cav2.3 or R-type channels can be blocked effectively by the peptide toxin SNX-482 (Newcomb *et al.*, 1998; Tottene *et al.*, 2000). Treatment of OB slices with 200 nM SNX-482 did not significantly alter the peak amplitude of ON-evoked M/T cell EPSCs (Fig. 3E and F) (98 ± 9% of control; *t*-test,  $t_{21} = 0.08$ –1.17,  $P = 0.25$ –0.93). Taken together, these combined results using established, subtype-specific Cav channel antagonists indicated a predominant role for presynaptic Cav2.2 channels in mediating fast synaptic transmission at mouse OSN axonal terminals.

#### Olfactory nerve-evoked excitatory postsynaptic currents persist in Cav2.2<sup>-/-</sup> mice

We next examined the effect of a targeted ablation of Cav2.2 on ON-evoked EPSCs in M/T cells (Fig. 4). We recorded EPSCs over time and compared M/T cell responses from Cav2.2<sup>+/-</sup> vs. Cav2.2<sup>-/-</sup> mice. In both cases, large EPSCs could be elicited (Fig. 4A–C). Peak amplitudes of EPSCs in Cav2.2<sup>+/-</sup> mice ranged between -190 pA and -1.5 nA, with an average size of  $-616 \pm 65$  pA ( $n = 25$ ), whereas those in Cav2.2<sup>-/-</sup> mice ranged between -100 pA and -1.8 nA, with an average size of  $-586 \pm 70$  pA ( $n = 33$ ). There was no significant difference between the two genotypes (Fig. 4C) (*t*-test,  $t_{56} = 0.30$ ,  $P = 0.76$ ). We also observed no significant differences between the two genotypes in the latency of EPSC onset following ON stimulation [Cav2.2<sup>+/-</sup>, 2.8 ± 0.19 ms (range: 1.7–3.8 ms),  $n = 11$ ; Cav2.2<sup>-/-</sup>, 2.6 ± 0.16 ms (range: 1.6–3.4 ms),  $n = 15$ ; *t*-test,  $t_{24} = 0.44$ ,  $P = 0.66$ ] or in the duration of EPSCs before returning to baseline (Cav2.2<sup>+/-</sup>, 1.32 ± 0.06 s,  $n = 11$ ; Cav2.2<sup>-/-</sup>, 1.18 ± 0.04 s,  $n = 12$ ; *t*-test,  $t_{21} = 0.30$ ,  $P = 0.77$ ; Fig. 4D and E).

Next, we determined whether EPSC activation thresholds had changed as a result of the Cav2.2<sup>-/-</sup> deletion. We analysed EPSC peak amplitudes as a function of ON stimulation strength between 10 and 100 V in Cav2.2<sup>+/-</sup> vs. Cav2.2<sup>-/-</sup> mice (Fig. 4A, B and F). Stimulation intensities of 10–20 V were sufficient to induce EPSCs in M/T cells of both genotypes (Fig. 4A, B and F). With increasing stimulus strengths, EPSC peak amplitudes of both genotypes rose to a maximum; there were no statistically significant differences in these curves between the two genotypes (Fig. 4F; *t*-test,  $t_{12} = 0.04$ –0.88,  $P = 0.4$ –0.97).

We also analysed the effect of the Cav2.2 deletion on the expression of specific OB markers and on *in vivo* OB activation but, again, found no obvious differences between Cav2.2<sup>+/-</sup> and Cav2.2<sup>-/-</sup> mice (Fig. 5). To visualise potential changes in OB organisation between Cav2.2<sup>+/-</sup> and Cav2.2<sup>-/-</sup> mice, we first conducted immunohistochemical analyses using two classical markers for the olfactory system, olfactory marker protein (Keller & Margolis, 1976) and vesicular glutamate transporter type 2 (Gabellec *et al.*, 2007; Fig. 5A–F). Olfactory marker protein expression was detected in both nerve and glomerular layers, and the level of signal intensity and overall OB structure were similar in Cav2.2<sup>+/-</sup> and Cav2.2<sup>-/-</sup> mice. The same was true when we tested the expression of vesicular glutamate transporter type 2 (Fig. 5C–F). Both genotypes showed the typical presynaptic restriction to the glomeruli of the MOB and AOB (Fig. 5E and F), without any obvious differences in glomerular organisation, size, or signal intensity. Thus, the deletion of Cav2.2 did not cause any obvious changes to the anatomical organisation of the MOB or AOB. Consistent with the synaptic transmission recorded in single M/T cells of Cav2.2<sup>+/-</sup> and

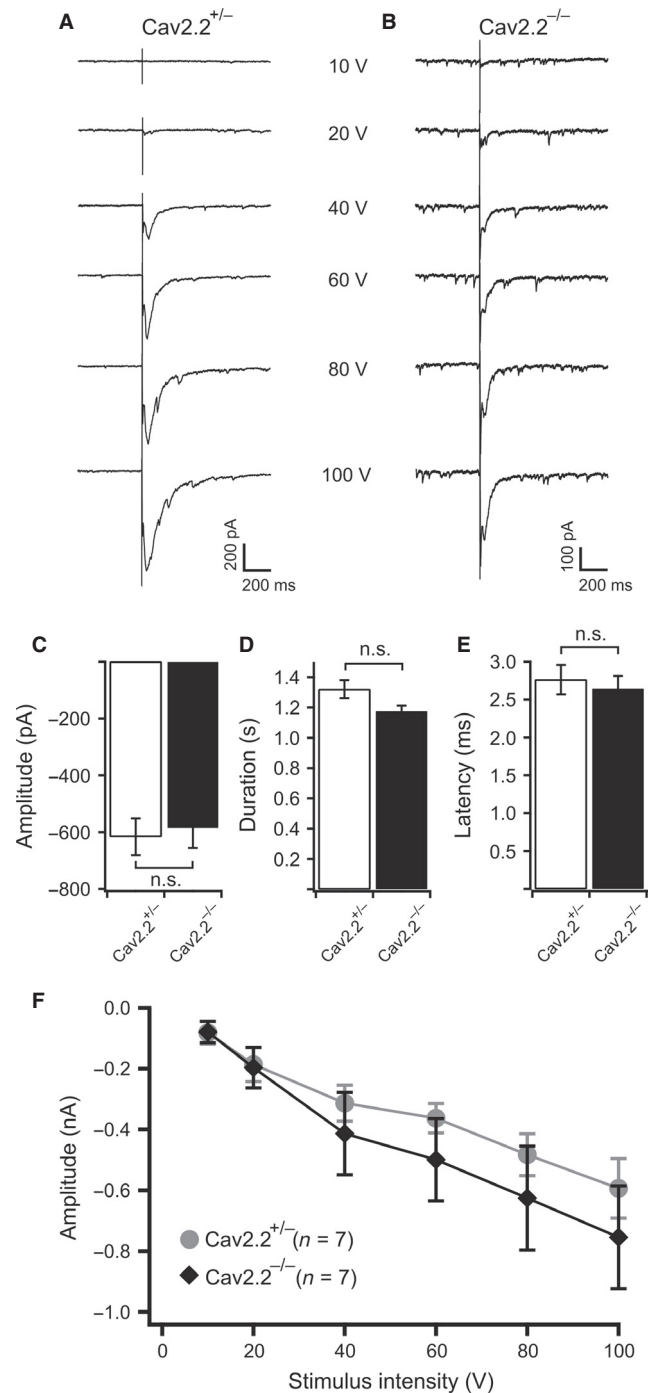


FIG. 4. There was no obvious difference in Cav2.2<sup>+/-</sup> vs. Cav2.2<sup>-/-</sup> mice in the dependence of ON-evoked EPSCs on synaptic strength. (A) Examples of EPSCs in a Cav2.2<sup>+/-</sup> M/T cell evoked by increasing electrical stimulus intensities. (B) EPSCs to increasing stimulus intensities recorded in a Cav2.2<sup>-/-</sup> M/T cell. Comparison of peak amplitudes (C), durations (D) and onset latencies (E) of ON-evoked EPSCs in M/T cells in Cav2.2<sup>+/-</sup> vs. Cav2.2<sup>-/-</sup> mice. (F) Peak EPSC amplitudes plotted as a function of stimulus intensity. Results are from seven M/T cells in each genotype.

Cav2.2<sup>-/-</sup> mice, the expression of TH in juxtglomerular neurons of the OB was indistinguishable between control and Cav2.2<sup>-/-</sup> mice (Fig. 5G–J). TH expression is dependent on afferent trans-synaptic activity and odour-stimulated glutamate release (Baker *et al.*, 1983), and was present throughout the whole OB. We obtained coronal OB sections of Cav2.2<sup>+/-</sup> ( $n = 3$ ) and Cav2.2<sup>-/-</sup> ( $n = 5$ )

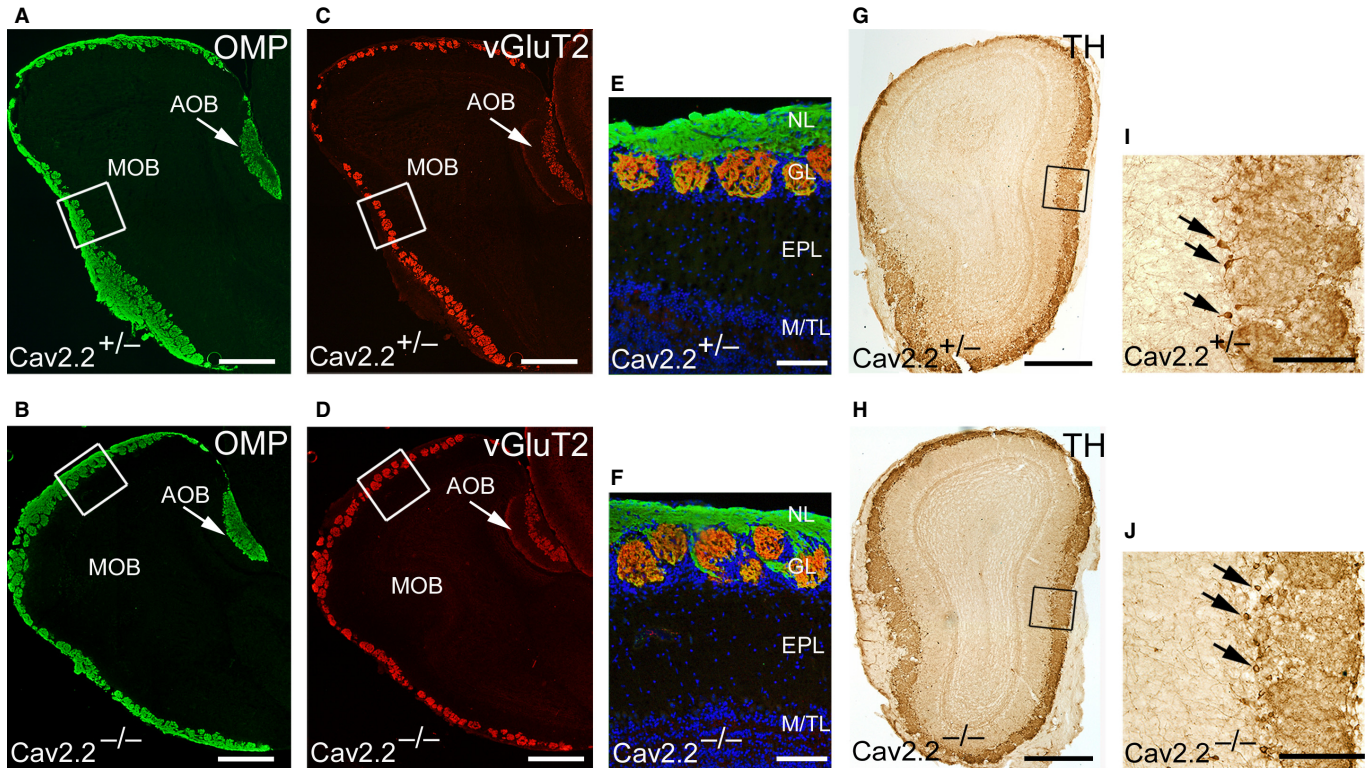


FIG. 5. Immunoreactivity for olfactory marker protein (OMP), vesicular glutamate transporter type 2 (vGluT2), and TH is unchanged in Cav2.2<sup>-/-</sup> mice. OMP immunoreactivity (green) detected in the OBs (12  $\mu$ m, sagittal plane) of (A) a Cav2.2<sup>+/-</sup> and (B) a Cav2.2<sup>-/-</sup> mouse is present in the MOB and AOB (arrow). (C, D) Immunoreactivity for the presynaptic marker vGluT2 (red) in the MOB and AOB (arrow) in the same sections. (E, F) Inset magnifications deriving from the co-localisation of OMP and vGluT2 from the boxed areas in A and C (Cav2.2<sup>+/-</sup>), and B and D (Cav2.2<sup>-/-</sup>). In both genotypes, OMP staining is present in the nerve layer (NL) and co-localises with vGluT2 solely in the glomerular layer (GL) (orange), whereas vGluT2 is absent in the NL. Nuclear counterstaining with Hoechst 33342 dye (blue) facilitates visualisation of MOB layers. EPL, external plexiform layer; M/TL, M/T cell layer. TH immunoreactivity (brown) in coronal sections of the MOB in Cav2.2<sup>+/-</sup> (G and I) and Cav2.2<sup>-/-</sup> (H and J) mice (2 months old). The inset magnifications (I and J) show that basal TH expression in juxtglomerular cells (arrows) is unchanged in Cav2.2<sup>-/-</sup> mice. Scale bars – 500  $\mu$ m (A–D, G and H); 100  $\mu$ m (insets, E, F, I and J).

mice and found equal levels of TH staining along the whole OB in both genotypes (Fig. 5G–J).

#### Olfactory nerve-evoked excitatory postsynaptic currents in Cav2.2<sup>-/-</sup> mice are resistant to voltage-activated calcium channel antagonists

The previous results established that targeted deletion of Cav2.2 did not cause a clear loss of synaptic transfer at ON axon terminals, unlike loss-of-function mutations in Nav1.7, which caused general anosmia (Weiss *et al.*, 2011). We next asked whether ON-evoked EPSCs in M/T cells of Cav2.2<sup>-/-</sup> mice exhibited altered pharmacological properties. We repeated experiments using  $\omega$ -conotoxin GVIA as a Cav2.2 antagonist and found that there was no effect of this treatment on EPSC peak amplitudes in Cav2.2<sup>-/-</sup> mice (Fig. 6A and D) (untreated,  $93 \pm 5\%$  of control,  $n = 6$ ;  $\omega$ -conotoxin GVIA,  $103 \pm 6\%$  of control,  $n = 7$ ;  $t$ -test,  $t_{11} = 0.1$ – $2.1$ ,  $P = 0.06$ – $0.93$ ), in marked contrast to the results obtained in B6 mice (see Fig. 2). Application of Cd<sup>2+</sup> (100  $\mu$ M) reduced the EPSC peak amplitudes to  $9 \pm 3\%$  in M/T cells of Cav2.2<sup>-/-</sup> mice ( $n = 4$ ) (Fig. 6C and E) ( $t$ -test,  $t_8 = 4.1$ – $11$ ,  $P < 0.004$  for stimulations 3–10), demonstrating that these currents still depended on high-voltage-gated Cav channels as in Fig. 1B. Hence, these experiments provided functional evidence that the Cav2.2 subunit was indeed absent from OSN axon terminals in Cav2.2<sup>-/-</sup> mice, yet they also indicated that considerable

reorganisation and compensation of Cav channel subunits must have occurred at these synapses as a result of the Cav2.2 deletion.

To gain insight into the question of which Cav subunits mediated OSN synaptic transfer to M/T cells in Cav2.2<sup>-/-</sup> mice, we performed further pharmacological analyses in these mice. We first tested the P/Q-type antagonist  $\omega$ -agatoxin IVA ( $n = 2$ ), the R-type antagonist SNX-482 ( $n = 3$ ), and the L-type antagonist nifedipine ( $n = 3$ ) but found virtually no effects of these compounds on ON-evoked EPSC peak amplitudes in M/T cells (data not shown). Next, we applied a combination of several antagonists known to block all major Cav channel subtypes (blocker mix: 200 nM  $\omega$ -agatoxin IVA, 200 nM SNX-482, 10  $\mu$ M nifedipine, 10  $\mu$ M mibefradil and 500  $\mu$ M Ni<sup>2+</sup>). Surprisingly, this treatment also did not have any significant effects on ON-evoked EPSC peak amplitudes in M/T cells of Cav2.2<sup>-/-</sup> mice (Fig. 6B and E) ( $83 \pm 11\%$  of control;  $n = 8$ ;  $t$ -test;  $t_{12} = 0.1$ – $2.01$ ,  $P = 0.07$ – $0.92$ ). Even with increased concentrations of these antagonists [ $\omega$ -agatoxin IVA/SNX-482, 400 nM each ( $n = 2$ ); nifedipine, 50  $\mu$ M ( $n = 2$ ); mibefradil, 50  $\mu$ M ( $n = 3$ )], none of the M/T cells showed a clear reduction in EPSC peak amplitude as a result of this treatment (data not shown). Taken together, our analysis of synaptic transmission at the first synapse in the mouse main olfactory pathway revealed that Cav2.2 was the predominant  $\alpha 1$  subunit at OSN presynaptic axon terminals and that a loss of Cav2.2 can be compensated by as yet undefined, blocker-resistant Cav channels.

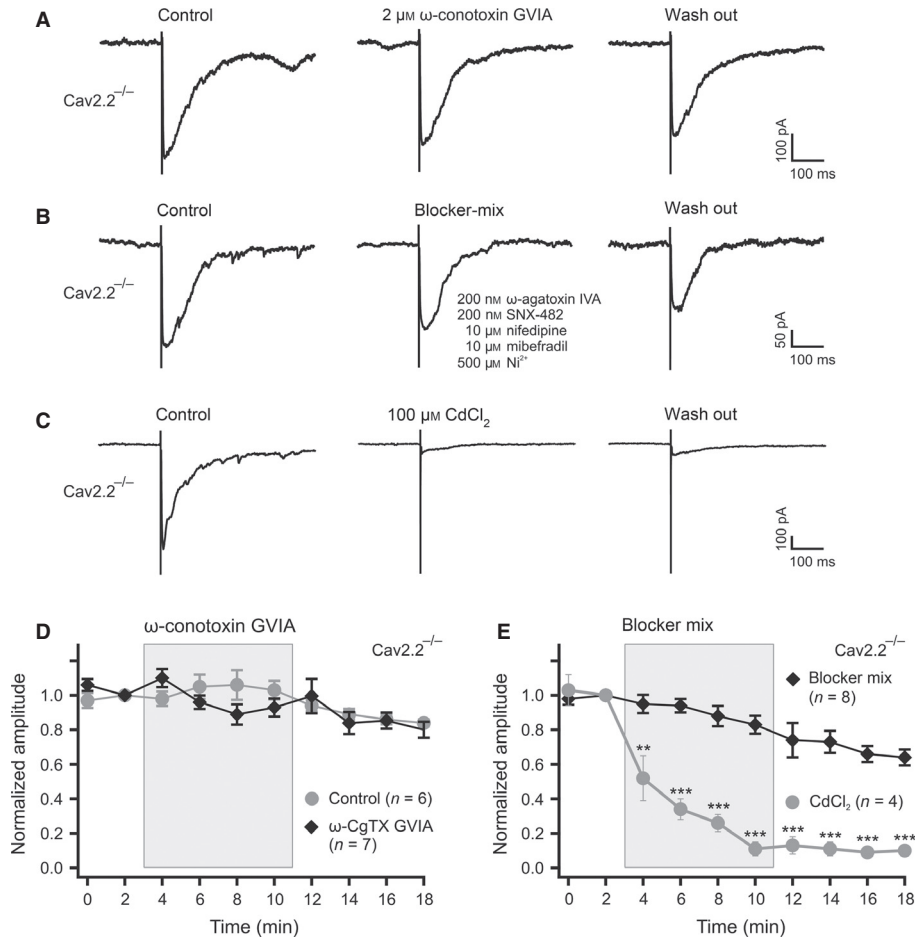


FIG. 6. ON-evoked EPSCs in Cav2.2<sup>-/-</sup> mice become resistant to a wide range of Ca<sup>2+</sup> channel antagonists. (A) EPSCs of an M/T cell of a Cav2.2<sup>-/-</sup> mouse treated with ω-conotoxin GVIA (2 μM). (B) EPSCs of an M/T cell of a Cav2.2<sup>-/-</sup> mouse treated with the Ca<sup>2+</sup> channel antagonists ω-agatoxin IVA (200 nM), SNX-482 (200 nM), nifedipine (10 μM), mibefradil (10 μM) and Ni<sup>2+</sup> (500 μM). (C) EPSCs of an M/T cell of a Cav2.2<sup>-/-</sup> mouse treated with CdCl<sub>2</sub> (100 μM). (D) Comparison of normalised EPSC peak amplitudes in Cav2.2<sup>-/-</sup> mice during application of ω-conotoxin GVIA (n = 7, black) and in untreated cells (n = 6, grey). (E) Normalised EPSC peak amplitudes in Cav2.2<sup>-/-</sup> mice during application of the blocker mix (n = 8, black) or Cd<sup>2+</sup> (n = 4, grey). \*\*P < 0.005; \*\*\*P < 0.0005.

#### Paired-pulse depression is severely impaired in Cav2.2<sup>-/-</sup> mice

Transmitter release from mammalian ON terminals onto postsynaptic cells showed a high level of paired-pulse depression (Murphy *et al.*, 2004; Tyler *et al.*, 2007) that is probably due to vesicle depletion and/or modulation of presynaptic Ca<sup>2+</sup> conductances (McGann *et al.*, 2005; Wachowiak *et al.*, 2005; Pirez & Wachowiak, 2008; McGann, 2013). To determine whether Cav2.2 played a role in this form of synaptic plasticity, we performed ON double-stimulation experiments using interstimulus intervals (ISIs) ranging between 30 and 5000 ms, and then quantified the paired-pulse ratio of peak amplitudes (EPSC<sub>2</sub> : EPSC<sub>1</sub>) in Cav2.2<sup>+/-</sup> vs. Cav2.2<sup>-/-</sup> mice. We found strong paired-pulse depression in M/T cells of Cav2.2<sup>+/-</sup> mice [Fig. 7A (top) and B]. EPSC peak amplitudes were greatly reduced at a 30-ms ISI between conditioning and test stimulus, with a mean paired-pulse ratio of 0.16 ± 0.03 (n = 7). With ISIs between 30 and 1000 ms, this ratio still remained below 0.5 and with an ISI of 5000 ms, the mean paired-pulse ratio reached 0.77 ± 0.04 (n = 7).

In M/T cells of Cav2.2<sup>-/-</sup> mice, these properties were clearly different and, overall, the extent of paired-pulse depression was strongly reduced [Fig. 7A (bottom) and B]. For example, with an ISI of 300 ms, paired-pulse ratios reached 0.6 ± 0.04 (n = 14) in

Cav2.2<sup>-/-</sup> mice vs. 0.32 ± 0.015 (n = 7) in Cav2.2<sup>+/-</sup> controls. Paired-pulse ratios differed significantly between the two genotypes at ISIs between 100 and 2000 ms (Fig. 7B) (*t*-test; ISI 100 ms, *t*<sub>18</sub> = 3.25, *P* < 0.005; ISI 300 ms, *t*<sub>20</sub> = 4.7, *P* < 0.0005; ISI 1000 ms, *t*<sub>20</sub> = 4.19, *P* < 0.0005; ISI 2000 ms, *t*<sub>19</sub> = 2.79, *P* < 0.05). Hence, the presence of a fully functional Cav2.2 subunit was essential for the expression of normal paired-pulse depression in ON-evoked synaptic responses of M/T cells.

#### Cav2.2 channels are required at vomeronasal nerve terminals in the accessory olfactory bulb for synaptic transmission to brief stimulation

Our immunohistochemical analyses of Cav2.2 expression in the olfactory system of Cav2.2<sup>+/-</sup> and Cav2.2<sup>-/-</sup> mice not only revealed the presence of this Cav channel subtype in MOB glomeruli of control tissue, but also showed strong expression in the glomerular layer of the AOB, suggesting a potential role for Cav2.2 in transmitter release from VN terminals (Fig. 2E–H). To test this possibility, we recorded EPSCs from mitral cells in the external plexiform layer of the AOB in response to VN-evoked electrical stimulation (Fig. 8). In Cav2.2<sup>+/-</sup> control mice, we recorded and

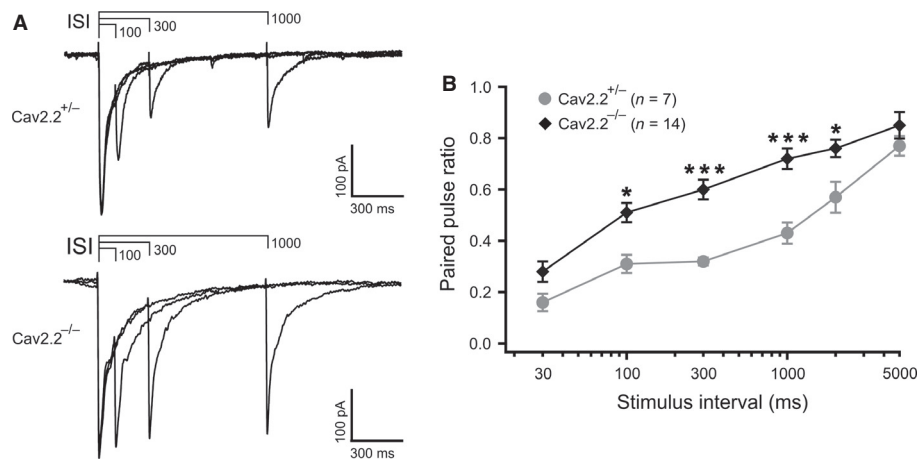


FIG. 7. Loss of Cav2.2 leads to decreased paired-pulse depression at OSN–M/T cell synapses. (A) Superimposed examples of ON-evoked EPSCs in Cav2.2<sup>+/−</sup> (upper panel) or Cav2.2<sup>−/−</sup> (lower panel) M/T cells in response to paired OSN stimulation using different ISIs (100, 300, and 1000 ms). Peak current amplitudes to the second pulse are reduced relative to the first pulse. (B) Paired-pulse ratios plotted as a function of ISI in Cav2.2<sup>+/−</sup> ( $n = 7$ , grey) and Cav2.2<sup>−/−</sup> ( $n = 14$ , black) animals. Error bars represent means  $\pm$  SEM. \* $P < 0.05$ ; \*\*\* $P < 0.0005$ .

analysed 22 AOB mitral cells (in seven animals). VN stimulation induced characteristic, transient inward currents with amplitudes ranging between  $-80$  and  $-750$  pA (mean  $-380 \pm 45$  pA;  $n = 15$ ) in response to a single 1-ms pulse (Fig. 8A). Evoked responses lasted between 0.6 and 2.9 s (mean  $1.5 \pm 0.2$  s;  $n = 14$ ). Compared with recordings from MOB M/T cells, the onset latency in AOB mitral cells after electrical stimulation was more than twice as long (AOB, mean  $5.8 \pm 0.5$  ms,  $n = 15$ ; MOB, mean  $2.8 \pm 0.19$  ms,  $n = 11$ ;  $t$ -test,  $t_{24} = 4.71$ ,  $P < 0.0005$ ). Importantly, application of  $\omega$ -conotoxin GVIA ( $2 \mu\text{M}$ ) nearly abolished peak amplitudes of VN-evoked EPSCs in AOB mitral cells (Fig. 8A and B) [ $8 \pm 4\%$  of control ( $n = 7$ );  $t$ -test,  $t_{15} = 3.6$ – $7.6$ ,  $P < 0.003$  for stimulations 6–10], whereas EPSC peak amplitudes of untreated cells ( $n = 9$ ) remained stable over time (Fig. 8B, grey) ( $89 \pm 9\%$  of control).

Next, we examined the effect of a loss of Cav2.2 on VN-evoked EPSCs in AOB mitral cells by comparing responses in slices from Cav2.2<sup>+/−</sup> vs. Cav2.2<sup>−/−</sup> mice (Fig. 8C and D). Results in Cav2.2<sup>−/−</sup> mice were based on 23 AOB mitral cells in eight animals. Strikingly, there was a nearly complete loss of postsynaptic response with brief, 1-ms stimulation in Cav2.2<sup>−/−</sup> mice. Both EPSC peak amplitudes (Cav2.2<sup>+/−</sup>, mean  $-380 \pm 45$  pA,  $n = 15$ ; Cav2.2<sup>−/−</sup>, mean  $50 \pm 11$  pA,  $n = 18$ ;  $t$ -test,  $t_{31} = 7.51$ ;  $P < 0.0005$ ) and durations (Cav2.2<sup>+/−</sup>, mean  $1.5 \pm 0.2$  s,  $n = 14$ ; Cav2.2<sup>−/−</sup>, mean  $0.16 \pm 0.03$  s,  $n = 16$ ;  $t$ -test,  $t_{28} = 7.50$ ;  $P < 0.0005$ ) were greatly diminished in Cav2.2<sup>−/−</sup> mice, whereas onset latencies, at least in those cells where residual responses could still be measured, were unchanged (Cav2.2<sup>+/−</sup>, mean  $5.8 \pm 0.5$  ms,  $n = 15$ ; Cav2.2<sup>−/−</sup>, mean  $6.8 \pm 0.3$  ms,  $n = 16$ ;  $t$ -test,  $t_{29} = 1.59$ ,  $P = 0.13$ ) (Fig. 8D). Thus, synaptic transmission at VN terminals in the AOB was sensitive to  $\omega$ -conotoxin GVIA and was highly diminished in Cav2.2<sup>−/−</sup> mice following VN stimulation with a single brief pulse. In contrast to the situation in the MOB, there seemed to be almost no or only very little  $\text{Ca}^{2+}$  channel compensation at these synapses after a loss of Cav2.2. We therefore concluded that Cav2.2 functioned as the predominant  $\alpha 1$  Cav channel subunit for fast synaptic transmission at these synapses.

However, we also found clear evidence for functional specialisation (Dietrich *et al.*, 2003) of additional Cav channel subunits at VN terminals, at least in a subset of the experiments. By using 100-ms tetanic stimulation (10 pulses at 100 Hz, each pulse lasting

1 ms), we tested the effects of repetitive, prolonged synaptic stimulation (Ukhanov *et al.*, 2007) on AOB mitral cell EPSCs in Cav2.2<sup>+/−</sup> vs. Cav2.2<sup>−/−</sup> mice. In Cav2.2<sup>+/−</sup> mitral cells, tetanic stimulation evoked similar EPSCs as with 1-ms stimulations in terms of amplitude (Fig. 9A, B and D; mean  $383 \pm 41$  pA;  $n = 15$ ;  $t$ -test,  $t_{28} = 0.04$ ,  $P = 0.97$ ) and onset latency (Fig. 9F) (mean  $6.6 \pm 0.7$  ms;  $n = 14$ ;  $t$ -test,  $t_{27} = 0.88$ ,  $P = 0.39$ ), but there was an increase in the average duration of EPSCs compared with 1-ms stimulation (Fig. 9E; mean  $2.8 \pm 0.4$  s;  $n = 14$ ;  $t$ -test,  $t_{27} = 3.25$ ,  $P = 0.003$ ). A different situation occurred in AOB mitral cells of Cav2.2<sup>−/−</sup> mice where we observed two major subtypes of mitral cell responses. Type 1 responses showed essentially no or only very small synaptic currents with tetanic stimulation, similar to what we observed with 1-ms pulses (Fig. 9A, type 1; Fig. 9C, black) ( $n = 9$ ). In type 2 responses, tetanic stimulation recruited considerable EPSCs despite the absence of Cav2.2 (Fig. 9A, type 2; Fig. 9C, grey) ( $n = 7$ ). Interestingly, onset latencies of type 2 responses in Cav2.2<sup>−/−</sup> mice were almost doubled compared with heterozygous controls (Fig. 9F), suggesting at least the possibility that network properties had changed in these responses as a result of the Cav2.2 deletion. Furthermore, in contrast to M/T cells in the MOB of Cav2.2<sup>−/−</sup> mice, type 2 responses were not resistant to the combination of antagonists known to block all major Cav channel subtypes (blocker mix: 200 nM  $\omega$ -agatoxin IVA, 200 nM SNX-482, 10  $\mu\text{M}$  nifedipine, 10  $\mu\text{M}$  mibefradil and 500  $\mu\text{M}$   $\text{Ni}^{2+}$ ). EPSCs in type 2 cells of Cav2.2<sup>−/−</sup> mice could be effectively reduced by the blocker mix to  $13 \pm 4\%$  ( $n = 5$ ) (Fig. 9A, type 2/blocker mix), demonstrating that these remaining currents depended on Cav channels.

In summary, we concluded that Cav2.2 played a central role for fast synaptic transmission at VSN axon terminals. In the absence of Cav2.2, tetanic stimulation can recruit additional Cav channels with as yet unknown properties in at least a subset of the recorded cells. Although our pharmacological experiments have indicated critical roles for Cav2.2 at both olfactory and VN terminals, our analyses of Cav2.2<sup>−/−</sup> mice revealed distinct and unexpected differences in synaptic transmission at OSN and VSN axon terminals as a result of a loss of Cav2.2. These physiological differences probably reflect different functional constraints of the main and accessory olfactory systems.

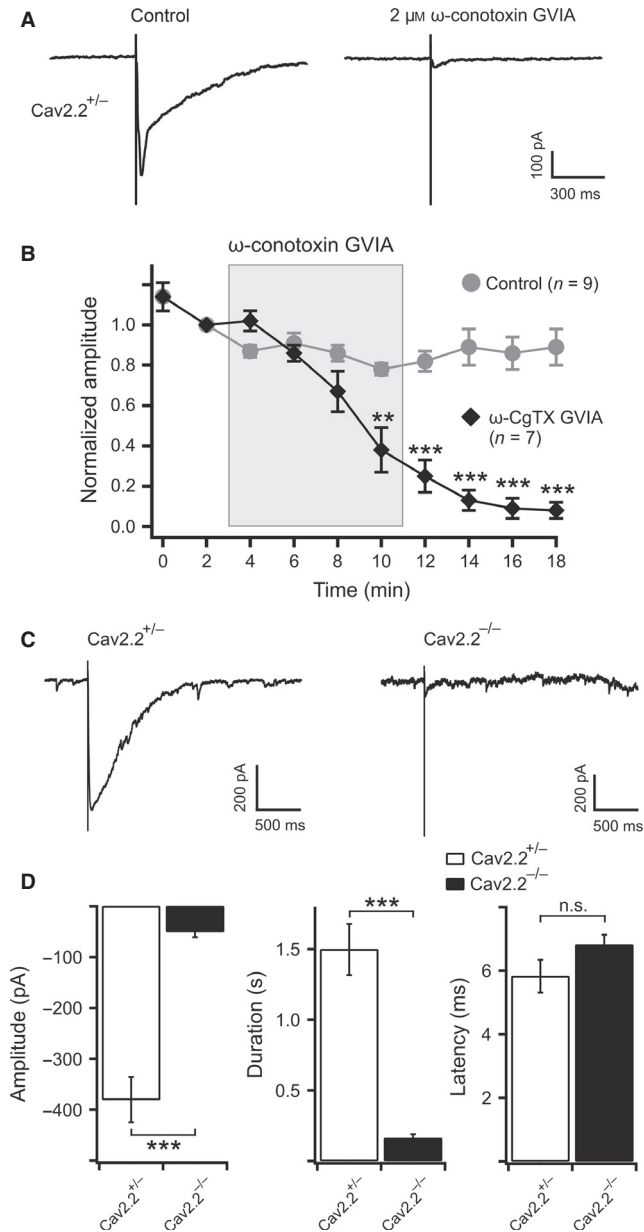


**FIG. 8.** Cav2.2 is required for VN-evoked synaptic transmission to brief stimulation. (A) Examples of EPSCs of an AOB mitral cell before (left) and during (right) treatment with  $\omega$ -conotoxin GVIA ( $2 \mu\text{M}$ ). (B) Normalised peak EPSC amplitudes of control cells ( $n = 9$ , grey) vs. mitral cells treated with  $\omega$ -conotoxin (CgTX) GVIA ( $n = 7$ , black). (C) Representative EPSCs of AOB mitral cells in Cav2.2<sup>+/-</sup> (left) and Cav2.2<sup>-/-</sup> (right) mice to brief 1-ms VN stimulation. (D) Comparison of peak amplitudes (left), durations (middle) and onset latencies (right) of VN-evoked EPSCs in AOB mitral cells of Cav2.2<sup>+/-</sup> vs. Cav2.2<sup>-/-</sup> mice. \*\* $P < 0.005$ ; \*\*\* $P < 0.0005$ .

## Discussion

This study describes novel aspects of the function of Cav channels for synaptic transmission at mouse olfactory and VN terminals. Our experiments provide three converging lines of evidence indicating a central role of the N-type subunit Cav2.2 in transmitter release at the first synapse of the main and accessory olfactory pathways, respectively. First, our immunohistochemical experiments have localised striking Cav2.2 immunoreactivity to the glomerular neuropil of the MOB and AOB. This immunoreactivity is absent in

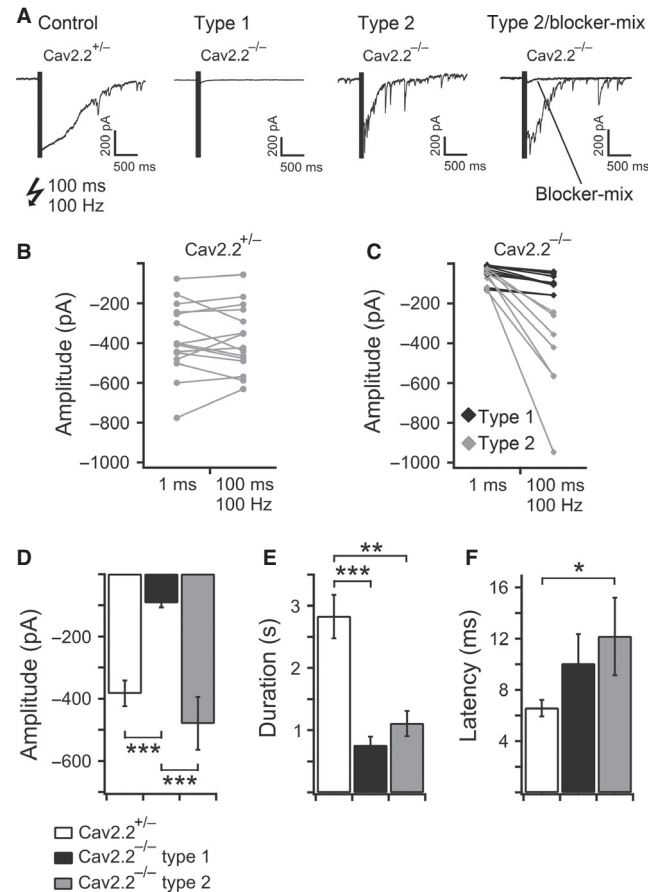


**FIG. 9.** Differential effects of VN tetanic stimulation on AOB synaptic transmission in Cav2.2<sup>+/-</sup> and Cav2.2<sup>-/-</sup> mice. (A) Examples of EPSCs of AOB mitral cells in Cav2.2<sup>+/-</sup> (control) and Cav2.2<sup>-/-</sup> (type 1 and type 2) mice to tetanic stimulation. Type 2 cell responses were sensitive to Cav channel antagonists (type 2/blocker mix). (B) Comparison of EPSC peak amplitudes of individual cells recorded in Cav2.2<sup>+/-</sup> mice. EPSCs were first generated by a 1-ms pulse and subsequently by tetanic (100 Hz) stimulation. (C) EPSC peak amplitudes to 1-ms vs. tetanic stimulations of all cells recorded in Cav2.2<sup>-/-</sup> mice. Cells were grouped into type 1 cells (black, peak amplitude ratios EPSC<sub>short pulse</sub> : EPSC<sub>tetanic</sub> > 0.25) and type 2 cells (grey, peak amplitude ratios EPSC<sub>short pulse</sub> : EPSC<sub>tetanic</sub> < 0.25). Comparison of peak amplitudes (D), durations (E) and onset latencies (F) of VN-evoked EPSCs to tetanic stimulations in Cav2.2<sup>+/-</sup> mice vs. type 1 (black) and type 2 (grey) cells in Cav2.2<sup>-/-</sup> mice. \* $P < 0.05$ ; \*\* $P < 0.005$ ; \*\*\* $P < 0.0005$ .

Cav2.2<sup>-/-</sup> mice, thus validating the specificity of the staining. Furthermore, it co-localises with molecules of the presynaptic active zone, such as bassoon and vesicular glutamate transporter type 2 in Cav2.2<sup>+/-</sup> mice, but is absent from olfactory or VN layers. Second, our voltage-clamp recordings of ON- or VN-evoked EPSCs in M/T and superficial tufted cells (STCs) of the MOB and mitral cells of the AOB, in combination with the use of subtype-specific Cav channel antagonists, provide clear evidence of a predominant role of N-type Cav channels in transmitter release at these synapses. Effective voltage clamp of postsynaptic dendrites at negative membrane potentials ruled out a contribution of high-voltage-gated Cav channels in postsynaptic mitral cell dendrites (Normann *et al.*, 2000; Yuan *et al.*, 2004). Third, voltage-clamp recordings in Cav2.2<sup>-/-</sup> mice demonstrate that the properties of synaptic transmission at OSN axon terminals are clearly altered in these mice. Following a loss of Cav2.2, M/T cell EPSCs are rendered blocker-resistant, thus indicating a major reorganisation and compensation of Cav channel

subunits as a result of the Cav2.2 deletion at this synapse. Our experiments in Cav2.2<sup>-/-</sup> mice also reveal that Cav2.2 is critically required for paired-pulse depression of ON-evoked EPSCs in M/T cells of the MOB, and they demonstrate an essential role for Cav2.2 in VN-evoked EPSCs of AOB mitral cells. To the best of our knowledge, this is the first report investigating the effects of a Cav channel mutation on synaptic transmission in the mammalian olfactory system.

Our findings are supported by previous results. Using calcium imaging at OSN axon terminals, single ON nerve shocks evoked fluorescence increases that were largely blocked by  $\omega$ -conotoxin GVIA (Wachowiak *et al.*, 2005). The same study showed that presynaptic calcium influx via N-type Cav channels at ON axon terminals can be regulated and suppressed by GABAergic interneurons, leading to presynaptic inhibition of OSN input to MOB glomeruli (Wachowiak *et al.*, 2005). Our results at VSN axon terminals in the AOB are also broadly consistent with a study that employed Fos immunoreactivity to demonstrate that pheromonal activation of AOB periglomerular cells was reduced in Cav2.2-deficient mice (Murakami *et al.*, 2006). However, no direct measurements of VN-evoked synaptic transmission were obtained in this work.

Recent work has provided evidence that MOB mitral cells are excited through a multistep signalling path involving direct OSN-tufted cell excitation followed by feedforward excitation through tufted cell-mitral cell synaptic connections (De Saint Jan *et al.*, 2009; Gire *et al.*, 2012). Although we used special precautions to minimise direct electrical stimulation of tufted cell dendrites, performed recordings on both sTCs and M/T cells, and observed short EPSC latencies and rapid rise times under our recording conditions, our experiments do not strictly differentiate between direct OSN-mitral cell transmission and OSN-mitral cell transmission that is indirect via tufted cell dendrites. Future experiments, perhaps using optogenetic stimulation of OSN axons, will be required to address this issue. Nonetheless, our work clearly demonstrates that N-type Cav channels are the main contributors to the presynaptic release in both olfactory and VN terminals.

The mammalian main olfactory system retains a high level of plasticity throughout life (Cheetham & Belluscio, 2014) and can detect an almost unlimited number of odour cues (Bushdid *et al.*, 2014). The accessory olfactory system is thought to function as a hardwired system that regulates a variety of innate, pheromone-evoked behavioural responses (Dulac & Wagner, 2006; Chamero *et al.*, 2012), although there is also clear evidence for learned behaviours in the accessory system (Brennan & Zufall, 2006; Roberts *et al.*, 2012; Oboti *et al.*, 2014) as well as integration and experience-dependent survival of newly generated neurons in AOB circuits (Oboti *et al.*, 2011). An unexpected result of the present study is that ablation of Cav2.2 causes differential consequences for neurotransmission at sensory nerve terminals in the MOB and AOB. In the MOB, we find that ablation of Cav2.2 does not eliminate ON-evoked EPSCs in M/T cells, yet this procedure does abolish sensitivity for the N-type blocker  $\omega$ -conotoxin GVIA (Fig. 6). By contrast, we find VN-evoked mitral cell EPSCs in the AOB to be absent or strongly reduced in Cav2.2<sup>-/-</sup> mice, at least with single nerve stimulation (Fig. 8). Thus, primary synapses in these two olfactory subsystems react differently to a loss of Cav2.2. Although we cannot yet determine the underlying causes and mechanisms for this differential Cav channel regulation, these two types of synapses could become a useful model for investigating the differential regulation, plasticity, and compensatory function of presynaptic Cav channels at mammalian nerve terminals. In an attempt to determine the pharmacological properties of the remaining calcium channels

underlying transmitter release at ON nerve terminals of Cav2.2<sup>-/-</sup> mice, we find that EPSCs become resistant to virtually all known Cav channel toxins as a result of a loss of Cav2.2, yet they can still be blocked by Cd<sup>2+</sup>. Thus, pharmacologically, the remaining calcium channels behaved as non-L-type, non-P/Q-type, non-R-type, non-T-type, and non-N-type Cav channels, indicating clear compensatory alteration of synaptic transmission in Cav2.2<sup>-/-</sup> mice. Defining the molecular nature of these toxin-resistant channels remains a goal for future research but there is a precedent for the existence of such channels in the nervous system. Blocker-resistant presynaptic Cav channels have been described in the nucleus of the solitary tract (Yamazaki *et al.*, 2006) and in glutamatergic excitatory synaptic transmission of the anterior cingulate cortex (Kang *et al.*, 2013).

Initially, our main motivation for this investigation was to gain insight into the question of whether presynaptic Cav channels at the first olfactory synapse could be rewarding targets for anosmia-related gene defects, equivalent to the consequences on olfaction by loss-of-function mutations in *Scn9a* (Weiss *et al.*, 2011). Our findings indicate that a loss of Cav2.2 is unlikely to cause general anosmia, at least in mice, due to the remarkable plasticity and compensation abilities of the first synapse in the main olfactory pathway. Although it is unknown whether the human olfactory system would show equally plastic capabilities, we predict that a loss-of-function mutation in *CACNA1B* would not cause general anosmia in humans, and our results in the mouse AOB are not relevant for human olfaction as the human accessory system is thought to be non-functional (Brennan & Zufall, 2006). Nonetheless, global ablation of Cav2.2 has revealed a highly interesting behavioural phenotype in Cav2.2<sup>-/-</sup> mice. These animals show markedly enhanced aggressive behaviours to an intruder mouse in the resident-intruder test, thus establishing hyperaggressive social behaviours in Cav2.2<sup>-/-</sup> males (Kim *et al.*, 2009). This result is remarkable in the light of previous findings showing that mutations of critical signalling molecules in both the main olfactory epithelium (Mandiyan *et al.*, 2005) and vomeronasal organ (Leypold *et al.*, 2002; Stowers *et al.*, 2002; Chamero *et al.*, 2011; Leinders-Zufall *et al.*, 2014) strongly affect the display of social aggression in male and female mice. Furthermore, there is currently enhanced interest in establishing a genetic basis for general olfactory sensitivity (Keydar *et al.*, 2013). Although Kim *et al.* (2009) have provided some evidence that the hyperaggressive phenotype of Cav2.2<sup>-/-</sup> mice is associated with altered neuronal activity in the dorsal raphe nucleus, it cannot be ruled out at present that altered synaptic function in the olfactory system as described here could also contribute to hyperaggression in Cav2.2<sup>-/-</sup> mice. To test this idea, it will be necessary to generate mice with a conditional, cell-type specific ablation of Cav2.2, similar to the approach that we developed for Nav1.7 (Weiss *et al.*, 2011) and the G protein G $\alpha$  (Chamero *et al.*, 2011; Oboti *et al.*, 2014).

The Cav2.2-deficient mouse models were generated 13 years ago independently by three groups (Ino *et al.*, 2001; Kim *et al.*, 2001; Saegusa *et al.*, 2001). Although the Cav2.2 channel is widely recognised for its important contribution to presynaptic Ca<sup>2+</sup> influx at many synapses of the nervous system, well-defined neurological phenotypes in these mouse mutants have been sparse, with the clearest effects in the pain system and at sympathetic nerve terminals (Striessnig & Koschak, 2008). Our results identifying altered synaptic transmission in the olfactory system of Cav2.2-deficient mice suggest that the olfactory system could become an attractive model to learn more about this channel and the consequences of its removal. Cav2.2-deficient mice should also be useful for future analyses of glomerular microcircuits in the MOB and AOB.

## Acknowledgements

We thank Y. Mori (Kyoto University) for providing Cav2.2-deficient mice and V. Flockerzi for valuable advice on this project. P. Hammes provided expert technical assistance. This work was supported by Deutsche Forschungsgemeinschaft Grants Sonderforschungsbereich 894/A17 (to F.Z.), 894/P2 (to P.W.), and PY90/1-1 (to M.P.). J.W. is the recipient of a HOM-FOR2012 Award from the University of Saarland.

## Conflict of interest

The authors declare that there was no conflict of interest.

## Abbreviations

AOB, accessory olfactory bulb; Cav, voltage-activated calcium; EPSC, excitatory postsynaptic current; ISI, interstimulus interval; MOB, main olfactory bulb; M/T, mitral/tufted; Nav, voltage-activated sodium; OB, olfactory bulb; ON, olfactory nerve; OSN, olfactory sensory neuron; PBS, phosphate-buffered saline; sTC, superficial tufted cell; TH, tyrosine hydroxylase; VN, vomeronasal nerve; VSN, vomeronasal sensory neuron.

## References

Baker, H., Kawano, T., Margolis, F.L. & Joh, T.H. (1983) Transneuronal regulation of tyrosine hydroxylase expression in olfactory bulb of mouse and rat. *J. Neurosci.*, **3**, 69–78.

Brennan, P.A. & Zufall, F. (2006) Pheromonal communication in vertebrates. *Nature*, **444**, 308–315.

Bushdid, C., Magnasco, M.O., Vosshall, L.B. & Keller, A. (2014) Humans can discriminate more than 1 trillion olfactory stimuli. *Science*, **343**, 1370–1372.

Carlson, G.C., Shipley, M.T. & Keller, A. (2000) Long-lasting depolarizations in mitral cells of the rat olfactory bulb. *J. Neurosci.*, **20**, 2011–2021.

Catterall, W.A., Goldin, A.L. & Waxman, S.G. (2005a) International Union of Pharmacology. XLVII. Nomenclature and structure-function relationships of voltage-gated sodium channels. *Pharmacol. Rev.*, **57**, 397–409.

Catterall, W.A., Perez-Reyes, E., Snutch, T.P. & Striessnig, J. (2005b) International Union of Pharmacology. XLVIII. Nomenclature and structure-function relationships of voltage-gated calcium channels. *Pharmacol. Rev.*, **57**, 411–425.

Chamero, P., Katsoulidou, V., Hendrix, P., Bufe, B., Roberts, R., Matsunami, H., Abramowitz, J., Birnbaumer, L., Zufall, F. & Leinders-Zufall, T. (2011) G protein Gao is essential for vomeronasal function and aggressive behavior in mice. *Proc. Natl. Acad. Sci. USA*, **108**, 12898–12903.

Chamero, P., Leinders-Zufall, T. & Zufall, F. (2012) From genes to social communication: molecular sensing by the vomeronasal organ. *Trends Neurosci.*, **35**, 597–606.

Cheetham, C.E. & Belluscio, L. (2014) Neuroscience. An olfactory critical period. *Science*, **344**, 157–158.

Christie, J.M., Bark, C., Hornmuzzi, S.G., Helbig, I., Monyer, H. & Westbrook, G.L. (2005) Connexin36 mediates spike synchrony in olfactory bulb glomeruli. *Neuron*, **46**, 761–772.

Cregg, R., Momin, A., Rugiero, F., Wood, J.N. & Zhao, J. (2010) Pain channelopathies. *J. Physiol.*, **588**, 1897–1904.

Dani, A., Huang, B., Bergan, J., Dulac, C. & Zhuang, X. (2010) Superresolution imaging of chemical synapses in the brain. *Neuron*, **68**, 843–856.

De Saint Jan, D., Hirnet, D., Westbrook, G.L. & Charpak, S. (2009) External tufted cells drive the output of olfactory bulb glomeruli. *J. Neurosci.*, **29**, 2043–2052.

tom Dieck, S., Sanmarti-Vila, L., Langnaese, K., Richter, K., Kindler, S., Soyke, A., Wex, H., Smalla, K.H., Kampf, U., Franzer, J.T., Stumm, M., Garner, C.C. & Gundelfinger, E.D. (1998) Bassoon, a novel zinc-finger CAG/glutamine-repeat protein selectively localized at the active zone of presynaptic nerve terminals. *J. Cell Biol.*, **142**, 499–509.

Dietrich, D., Kirschstein, T., Kukley, M., Pereverzev, A., von der Brélie, C., Schneider, T. & Beck, H. (2003) Functional specialization of presynaptic Ca<sub>v</sub>2.3 Ca<sup>2+</sup> channels. *Neuron*, **39**, 483–496.

Dulac, C. & Wagner, S. (2006) Genetic analysis of brain circuits underlying pheromone signaling. *Annu. Rev. Genet.*, **40**, 449–467.

Feldmesser, E., Bercovich, D., Avidan, N., Halbertal, S., Haim, L., Gross-Isseroff, R., Goshen, S. & Lancet, D. (2007) Mutations in olfactory signal

transduction genes are not a major cause of human congenital general anosmia. *Chem. Senses*, **32**, 21–30.

Gabellec, M.M., Panzanelli, P., Sassoe-Pognetto, M. & Lledo, P.M. (2007) Synapse-specific localization of vesicular glutamate transporters in the rat olfactory bulb. *Eur. J. Neurosci.*, **25**, 1373–1383.

Gire, D.H., Franks, K.M., Zak, J.D., Tanaka, K.F., Whitesell, J.D., Mulligan, A.A., Hen, R. & Schoppa, N.E. (2012) Mitral cells in the olfactory bulb are mainly excited through a multistep signaling path. *J. Neurosci.*, **32**, 2964–2975.

Habermann, C.J., O'Brien, B.J., Wässle, H. & Protti, D.A. (2003) AII amacrine cells express L-type calcium channels at their output synapses. *J. Neurosci.*, **23**, 6904–6913.

Hayar, A., Shipley, M.T. & Ennis, M. (2005) Olfactory bulb external tufted cells are synchronized by multiple intraglomerular mechanisms. *J. Neurosci.*, **25**, 8197–8208.

Ino, M., Yoshinaga, T., Wakamori, M., Miyamoto, N., Takahashi, E., Sonoda, J., Kagaya, T., Oki, T., Nagasu, T., Nishizawa, Y., Tanaka, I., Imoto, K., Aizawa, S., Koch, S., Schwartz, A., Niidome, T., Sawada, K. & Mori, Y. (2001) Functional disorders of the sympathetic nervous system in mice lacking the  $\alpha_{1B}$  subunit (Cav 2.2) of N-type calcium channels. *Proc. Natl. Acad. Sci. USA*, **98**, 5323–5328.

Isaacson, J.S. & Strowbridge, B.W. (1998) Olfactory reciprocal synapses: dendritic signaling in the CNS. *Neuron*, **20**, 749–761.

Kamp, M.A., Hanggi, D., Steiger, H.J. & Schneider, T. (2012) Diversity of presynaptic calcium channels displaying different synaptic properties. *Rev. Neuroscience*, **23**, 179–190.

Kang, S.J., Liu, M.G., Shi, T.Y., Zhao, M.G., Kaang, B.K. & Zhuo, M. (2013) N-type voltage gated calcium channels mediate excitatory synaptic transmission in the anterior cingulate cortex of adult mice. *Mol. Pain*, **9**, 58.

Karstensen, H.G. & Tommerup, N. (2012) Isolated and syndromic forms of congenital anosmia. *Clin. Genet.*, **81**, 210–215.

Keller, A. & Margolis, F.L. (1976) Isolation and characterization of rat olfactory marker protein. *J. Biol. Chem.*, **251**, 6232–6237.

Keydar, I., Ben-Asher, E., Feldmesser, E., Nativ, N., Oshimoto, A., Restrepo, D., Matsunami, H., Chien, M.S., Pinto, J.M., Gilad, Y., Olender, T. & Lancet, D. (2013) General olfactory sensitivity database (GOSdb): candidate genes and their genomic variations. *Hum. Mutat.*, **34**, 32–41.

Kim, C., Jun, K., Lee, T., Kim, S.S., McEnery, M.W., Chin, H., Kim, H.L., Park, J.M., Kim, D.K., Jung, S.J., Kim, J. & Shin, H.S. (2001) Altered nociceptive response in mice deficient in the  $\alpha_{1B}$  subunit of the voltage-dependent calcium channel. *Mol. Cell. Neurosci.*, **18**, 235–245.

Kim, C., Jeon, D., Kim, Y.H., Lee, C.J., Kim, H. & Shin, H.S. (2009) Deletion of N-type Ca<sup>2+</sup> channel Cav2.2 results in hyperaggressive behaviors in mice. *J. Biol. Chem.*, **284**, 2738–2745.

Leinders-Zufall, T., Ishii, T., Chamero, P., Hendrix, P., Oboti, L., Schmid, A., Kircher, S., Pyrski, M., Akiyoshi, S., Khan, M., Vaes, E., Zufall, F. & Mombaerts, P. (2014) A family of nonclassical class I MHC genes contributes to ultrasensitive chemodetection by mouse vomeronasal sensory neurons. *J. Neurosci.*, **34**, 5121–5133.

Leybold, B.G., Yu, C.R., Leinders-Zufall, T., Kim, M.M., Zufall, F. & Axel, R. (2002) Altered sexual and social behaviors in trp2 mutant mice. *Proc. Natl. Acad. Sci. USA*, **99**, 6376–6381.

Mandiyag, V.S., Coats, J.K. & Shah, N.M. (2005) Deficits in sexual and aggressive behaviors in *Cnga2* mutant mice. *Nat. Neurosci.*, **8**, 1660–1662.

McGann, J.P. (2013) Presynaptic inhibition of olfactory sensory neurons: new mechanisms and potential functions. *Chem. Senses*, **38**, 459–474.

McGann, J.P., Pirez, N., Gainey, M.A., Muratore, C., Elias, A.S. & Wachowiak, M. (2005) Odorant representations are modulated by intra- but not interglomerular presynaptic inhibition of olfactory sensory neurons. *Neuron*, **48**, 1039–1053.

Michalakis, S., Shaltiel, L., Sothilingam, V., Koch, S., Schludi, V., Krause, S., Zeitz, C., Audo, I., Lancelot, M.E., Hamel, C., Meunier, I., Preising, M.N., Friedburg, C., Lorenz, B., Zabouri, N., Haverkamp, S., Garrido, M.G., Tanimoto, N., Seeliger, M.W., Biel, M. & Wahl-Schott, C.A. (2014) Mosaic synaptopathy and functional defects in Cav1.4 heterozygous mice and human carriers of CSNB2. *Hum. Mol. Genet.*, **23**, 1538–1550.

Munger, S.D., Leinders-Zufall, T. & Zufall, F. (2009) Subsystem organization of the mammalian sense of smell. *Annu. Rev. Physiol.*, **71**, 115–140.

Murakami, M., Matsui, H., Shiraiwa, T., Suzuki, T., Sasano, H., Takahashi, E. & Kashiwahanagi, M. (2006) Decreases in pheromonal responses at the accessory olfactory bulb of mice with a deficiency of the  $\alpha_{1B}$  or  $\beta_3$  subunits of voltage-dependent Ca<sup>2+</sup> channels. *Biol. Pharm. Bull.*, **29**, 437–442.

Murphy, G.J., Glickfeld, L.L., Balsen, Z. & Isaacson, J.S. (2004) Sensory neuron signaling to the brain: properties of transmitter release from olfactory nerve terminals. *J. Neurosci.*, **24**, 3023–3030.

- Najac, M., De Saint Jan, D., Reguero, L., Grandes, P. & Charpak, S. (2011) Monosynaptic and polysynaptic feed-forward inputs to mitral cells from olfactory sensory neurons. *J. Neurosci.*, **31**, 8722–8729.
- Newcomb, R., Szoke, B., Palma, A., Wang, G., Chen, X., Hopkins, W., Cong, R., Miller, J., Urge, L., Tarczy-Hornoch, K., Loo, J.A., Dooley, D.J., Nadasdi, L., Tsien, R.W., Lemos, J. & Miljanich, G. (1998) Selective peptide antagonist of the class E calcium channel from the venom of the tarantula *Hysterocrates gigas*. *Biochemistry*, **37**, 15353–15362.
- Nickell, M.D., Breheny, P., Stromberg, A.J. & McClintock, T.S. (2012) Genomics of mature and immature olfactory sensory neurons. *J. Comp. Neurol.*, **520**, 2608–2629.
- Normann, C., Peckys, D., Schulze, C.H., Walden, J., Jonas, P. & Bischofberger, J. (2000) Associative long-term depression in the hippocampus is dependent on postsynaptic N-type Ca<sup>2+</sup> channels. *J. Neurosci.*, **20**, 8290–8297.
- Oboti, L., Schellino, R., Giachino, C., Chamero, P., Pyrski, M., Leinders-Zufall, T., Zufall, F., Fasolo, A. & Peretto, P. (2011) Newborn interneurons in the accessory olfactory bulb promote mate recognition in female mice. *Front. Neurosci.*, **5**, 113.
- Oboti, L., Pérez-Gómez, A., Keller, M., Jacobi, E., Birnbaumer, L., Leinders-Zufall, T., Zufall, F. & Chamero, P. (2014) A wide range of pheromone-stimulated sexual and reproductive behaviors in female mice depend on G protein G $\alpha$ . *BMC Biol.*, **12**, 31.
- Pirez, N. & Wachowiak, M. (2008) In vivo modulation of sensory input to the olfactory bulb by tonic and activity-dependent presynaptic inhibition of receptor neurons. *J. Neurosci.*, **28**, 6360–6371.
- Platzer, J., Engel, J., Schrott-Fischer, A., Stephan, K., Bova, S., Chen, H., Zheng, H. & Striessnig, J. (2000) Congenital deafness and sinoatrial node dysfunction in mice lacking class D L-type Ca<sup>2+</sup> channels. *Cell*, **102**, 89–97.
- Roberts, S.A., Davidson, A.J., McLean, L., Beynon, R.J. & Hurst, J.L. (2012) Pheromonal induction of spatial learning in mice. *Science*, **338**, 1462–1465.
- Saegusa, H., Kurihara, T., Zong, S., Kazuno, A., Matsuda, Y., Nonaka, T., Han, W., Toriyama, H. & Tanabe, T. (2001) Suppression of inflammatory and neuropathic pain symptoms in mice lacking the N-type Ca<sup>2+</sup> channel. *EMBO J.*, **20**, 2349–2356.
- Shepherd, G.M., Chen, W.R. & Greer, C.A. (2004) Olfactory bulb. In Shepherd, G.M. (Ed.), *The Synaptic Organization of the Brain*. Oxford University Press, Oxford, pp. 165–216.
- Stowers, L., Holy, T.E., Meister, M., Dulac, C. & Koentges, G. (2002) Loss of sex discrimination and male-male aggression in mice deficient for TRP2. *Science*, **295**, 1493–1500.
- Striessnig, J. & Koschak, A. (2008) Exploring the function and pharmacotherapeutic potential of voltage-gated Ca<sup>2+</sup> channels with gene knockout models. *Channels (Austin)*, **2**, 233–251.
- Striessnig, J., Bolz, H.J. & Koschak, A. (2010) Channelopathies in Ca<sub>v</sub>1.1, Ca<sub>v</sub>1.3, and Ca<sub>v</sub>1.4 voltage-gated L-type Ca<sup>2+</sup> channels. *Pflug. Arch. Eur. J. Phys.*, **460**, 361–374.
- Tottene, A., Volsen, S. & Pietrobon, D. (2000)  $\alpha_{1E}$  subunits form the pore of three cerebellar R-type calcium channels with different pharmacological and permeation properties. *J. Neurosci.*, **20**, 171–178.
- Tyler, W.J., Petzold, G.C., Pal, S.K. & Murthy, V.N. (2007) Experience-dependent modification of primary sensory synapses in the mammalian olfactory bulb. *J. Neurosci.*, **27**, 9427–9438.
- Ukhanov, K., Leinders-Zufall, T. & Zufall, F. (2007) Patch-clamp analysis of gene-targeted vomeronasal neurons expressing a defined V1r or V2r receptor: ionic mechanisms underlying persistent firing. *J. Neurophysiol.*, **98**, 2357–2369.
- Wachowiak, M., McGann, J.P., Heyward, P.M., Shao, Z., Puche, A.C. & Shipley, M.T. (2005) Inhibition [corrected] of olfactory receptor neuron input to olfactory bulb glomeruli mediated by suppression of presynaptic calcium influx. *J. Neurophysiol.*, **94**, 2700–2712.
- Waxman, S.G. & Zamponi, G.W. (2014) Regulating excitability of peripheral afferents: emerging ion channel targets. *Nat. Neurosci.*, **17**, 153–163.
- Weiss, J., Pyrski, M., Jacobi, E., Bufe, B., Willnecker, V., Schick, B., Zizzari, P., Gossage, S.J., Greer, C.A., Leinders-Zufall, T., Woods, C.G., Wood, J.N. & Zufall, F. (2011) Loss-of-function mutations in sodium channel Na<sub>v</sub>1.7 cause anosmia. *Nature*, **472**, 186–190.
- Yamazaki, K., Shigetomi, E., Ikeda, R., Nishida, M., Kiyonaka, S., Mori, Y. & Kato, F. (2006) Blocker-resistant presynaptic voltage-dependent Ca<sup>2+</sup> channels underlying glutamate release in mice nucleus tractus solitarii. *Brain Res.*, **1104**, 103–113.
- Yuan, Q., Mutoh, H., Debarbieux, F. & Knöpfel, T. (2004) Calcium signaling in mitral cell dendrites of olfactory bulbs of neonatal rats and mice during olfactory nerve stimulation and beta-adrenoceptor activation. *Learn. Memory*, **11**, 406–411.
- Zamponi, G.W., Lewis, R.J., Todorovic, S.M., Arneric, S.P. & Snutch, T.P. (2009) Role of voltage-gated calcium channels in ascending pain pathways. *Brain Res. Rev.*, **60**, 84–89.
- Zufall, F. (2005) Connexins and olfactory synchronicity: toward the olfactory code. *Neuron*, **46**, 693–694.
- Zufall, F., Pyrski, M., Weiss, J. & Leinders-Zufall, T. (2012) Link between pain and olfaction in an inherited sodium channelopathy. *Arch. Neurol.*, **69**, 1119–1123.